

UNIVERSITY OF TWENTE

Transducers Science and Technology Group

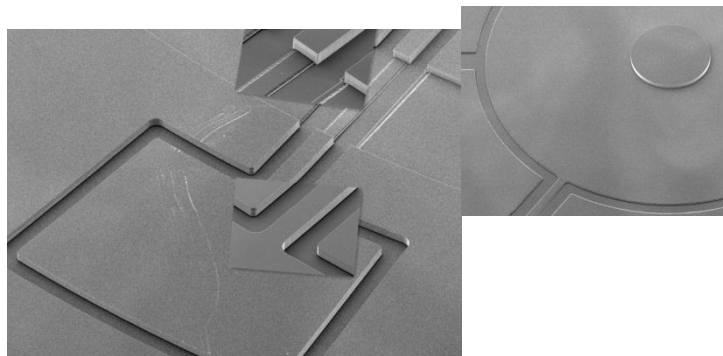
# Design, Fabrication and Characterization of a Piezo-electric Micro Control Valve

---

## Master Thesis Report

Kai Wu (s1227777)

*Electrical Engineering*



Supervising Committee: Prof. dr. ir. G. J. M. Krijnen  
Dr. ir. R. J. Wiegerink  
M. S. Groen, Msc  
Dr. ir. J. C. Lötters  
Dr. ir. D. M. Brouwer

12/02/2014



## CONTENTS

Abstract .....	3
Chapter 1 Introduction.....	4
1.1 Background .....	4
1.2 Thesis description.....	5
1.3 Thesis outline .....	6
Chapter 2 Previous microvalve.....	7
2.1 Introduction .....	7
2.2 Design and fabrication .....	7
2.3 Characterization of the piezo actuator.....	9
2.4 The first assembly .....	12
2.5 Measurement setup.....	13
2.6 Characterization .....	14
2.6 Conclusion .....	15
Chapter 3 New microvalve design.....	16
3.1 Conceptual Design.....	16
3.1.1 SOI wafer design.....	16
3.1.2 Glass wafer design.....	17
3.2 Dimensioning .....	18
3.2.1 Reference review.....	18
3.2.1 Flow model simulation.....	20
3.2.3 Valve membrane simulation.....	23
3.3 Summary .....	24
Chapter 4 New microvalve fabrication.....	26
4.1 Fabrication on the SOI wafer.....	26
4.1.1 Fabrication process .....	26
4.1.2 Liquid HF etching experimental results.....	28
4.1.3 DRIE experimental results .....	30
4.2 Fabrication on the glass wafer .....	33
4.2.1 Fabrication process .....	33
4.2.2 Powderblasting experimental results.....	33
4.3 Anodic bonding .....	35
4.3.1 Fabrication process .....	35
4.3.2 Anodic bonding .....	35
4.4 Conclusion .....	36
Chapter 5 Conclusions and recommendations .....	37
5.1 Previous piezo control microvalve.....	37
5.2 New microvalve.....	37
5.3 Future work.....	38
References.....	39
Acknowledgements.....	41

# Abstract

---

This master project consists of two sections. The first part is about assembling a miniature piezo actuator on an existing microvalve fabricated using a SOI (Silicon on Insulator) wafer, so the valve can be actuated piezoelectrically. After an introduction of development of microvalves since the last a few decades, the microvalve design and fabrication are reviewed. After that, the piezo actuator which will be mounted is tested separately in terms of acquainting its hysteresis curve. Besides, the work of assembling the microvalve and the piezo actuator is shown. In order to minimize the piezo hysteresis influence during the valve characterization, built-in capacitive displacement sensing is used to characterize the flow behavior under different gas flow pressures. Lastly, the difficulties from the assembly are summarized.

The second part deals with improving the valve design for direct assembly of a piezoelectric actuator onto the valve chip, allowing for easier assembly and better performance. At the beginning, the new SOI-based microvalve conceptual design is presented, which is required to be working under the certain conditions. To allow fluidic connections during the measurement, a bonded glass wafer is needed. Dimensioning the new valve is based on a radial flow model, and mechanical simulation of the valve membrane is demonstrated. After DRIE (Deep Reactive Ion Etching), HF etching, powderblasting; the new microvalve has been almost achieved. Meanwhile, experimental results from liquid HF etching, DRIE and powderblasting are shown and analyzed. Finally, conclusions about the previous microvalve and the new developed one are summarized, and some worthwhile future works are also suggested.

# Chapter 1 Introduction

---

*In this chapter, a general background information of the application is introduced first, and then this master thesis description is given after which the outline of this project is shown.*

## 1.1 Background

Since a few decades there have been an increasing number of people suffering from cardiovascular diseases worldwide, and monitoring patient's blood pressure waveform is of necessity during assessing these diseases. In particular, screening a continuous, accurate and real-time blood pressure waveform is more important when patients are diagnosed in the first-aid. Thus, many medical research institutes and companies have dedicated significant budgets to blood pressure measurement products.

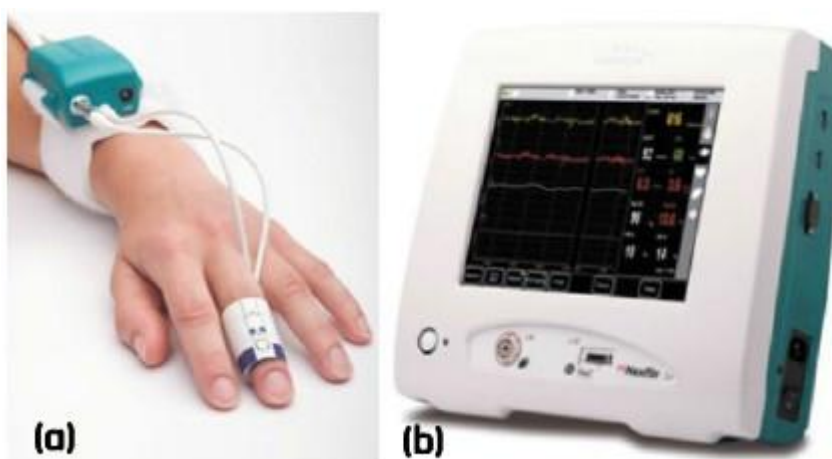


Figure 1.1: Demonstration of noninvasive and beat-to-beat arterial pressure monitoring systems. (a) The finger cuff consists of a photoplethysmograph (the ccNexfin System); (b) Immediate and reliable hemodynamic monitor [1].

Among many blood pressure monitoring techniques, noninvasive blood pressure measurement have become increasingly common in clinics and home care [2] In 1973, Peñáz described a noninvasive approach of measuring beat-to-beat blood pressure, and it did not incur the risk of arterial catheterization but could still offer the benefits of continuous blood pressure monitoring compared to invasive blood pressure measurement [3]. Figure 1.1 shows a noninvasive and real-time blood pressure monitoring device, and it is a good example to express Peñáz's idea of "vascular unloading" [4]. The primary measuring part is a photoelectric plethysmograph equipped with an inflatable cuff (a light source on one side of the cuff and infrared receiver on the opposite side); and it can estimate the blood volume of the finger via absorbing the infrared light, which is used in a feedback loop to adjust the cuff in order to maintain blood volume

constant and the vessels in a constant state of “vascular unloading” (Figure 1.1 (a)). This technique has been first modified in the 1990s during the “Finapres” (an acronym for FINGER Arterial PRESSure) project in the 1990s. It is assumed that the cuff pressure equals arterial pressure and brachial artery pressures are then reconstructed mathematically. This result of noninvasive method showed a similar waveform obtained from invasive arterial monitoring [5].

## 1.2 Thesis description

This master thesis project is mainly about a SOI-based microvalve with piezoelectric control, for application in ambulant, real-time blood pressure waveform monitoring systems based on a noninvasive method of measuring beat-to-beat blood pressure. The objective of using the SOI wafer is that its micromachining process is simpler compared to a general wafer. The working principle of this application is almost the same as previously described, but here the microvalve is the more attractive part. Using capacitive displacement sensing of the microvalve, capable of significantly minimizing the hysteresis impact induced from the mounted piezo actuator, is to control a microfluidic (nitrogen) system to allow the finger sleeve keeping blood volume constant. Likewise, the blood volume is estimated by measuring the finger’s photo-transparency via the LED light absorbance of the photocell (Figure 1.2).

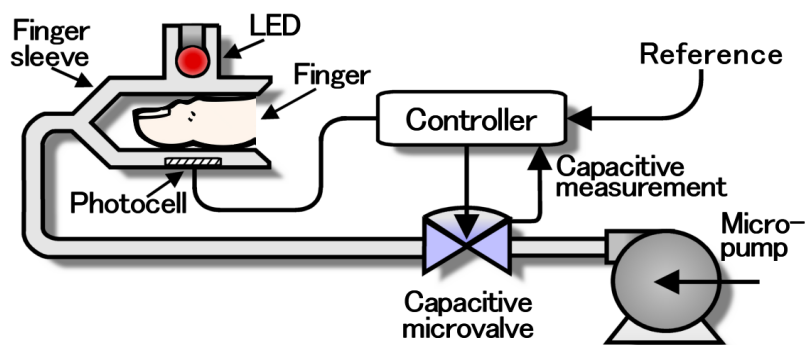


Figure 1.2: Application of the capacitive microvalve in a miniature blood pressure sensing device. The microvalve controls flow (nitrogen) to maintain the photocurrent as the same as the reference [6].

As the requirements of this application, the microvalve should be able to open and close stably and continuously in terms of controlling the gas flow volume. One critical part of this project is how to piezoelectrically actuate the microvalve, and mounting a piezo actuator on the microvalve becomes a practical issue. There are two kinds of microvalves which will be used. The first used was designed and fabricated by M. S. Groen *et al.* [6], and the redesign and the fabrication of the new microvalve are also major sections of this master thesis and they will be presented in the later chapters. The pressure drop across the new microvalve inlet and outlet should be smaller than 1 bar, and the volume flow is designed to be higher than 100 sccm (Standard Cubic Centimeters per Minute).

## **1.3 Thesis outline**

This thesis report will start with the microvalve design and fabrication, and characterization of the piezo actuator is then presented in Chapter 2. Moreover the assembly process of the piezo actuator and the microvalve will be given. Additionally, Chapter 2 describes the measurement setup of the assembling device and characterization results are discussed at the end.

As some difficulties are found during the first assembly, the microvalve is redesigned and it is described in Chapter 3. This chapter includes the new valve structure and its simulation in COMSOL Multiphysics. Based on the simulation results, the optimal valve dimensions can be determined. In the fourth chapter, the fabrication process of the new microvalve is shown as well as some results from the actual fabrication. Lastly, Chapter 5 summarizes the work which has been done and gives some recommendations on future work.

# Chapter 2 Previous microvalve

---

*This chapter firstly introduces the background of microvalves, and then gives an overview of the design and the fabrication for the previous microvalve which will be mounted with a piezo actuator. Then the piezo actuator and the whole assembly device are characterized, respectively. The flow behavior is discussed at the end.*

## 2.1 Introduction

Over the last several decades, microvalves have experienced a significant development because they have the advantages of a finer control rate, relatively faster response, lower production cost, smaller size and lower power consumption compared to traditional valves [7]. Due to various micromachining processes, microvalves can be fabricated in diverse materials resulting in valves for different applications. Specifically, most of the valves are made out of silicon with production processes based on MEMS (MicroElectroMechanical Systems) technology [8].

The microvalve can be actuated by a wide range of methods; for example, electrostatic, piezoelectrically, thermo-pneumatically, and thermo-mechanically and so on. Electrostatic actuation is limited in its deflection for large actuation force with low voltage because the generated electrostatic force between two parallel electrodes scales inversely with their spacing. For thermal actuation, despite of large stroke and actuation force are gained, it exhibits larger power consumption and longer response time [9]. In this thesis design, piezo actuation is taken into account as it is robust, capable of generating large forces even in small dimensions and consumes power only during the switching process [8]. Although hysteresis is the drawback of piezo actuators, the built-in capacitive displacement sensing is used to minimize it in this design.

## 2.2 Design and fabrication

The SOI-based microvalve has been successfully manufactured using simpler micromachining process compared to other microvalves [10]. The microvalve which will be used to assemble with the piezo actuator was designed and fabricated by M. S. Groen *et al.* (Figure 2.1) [6]. This microvalve is fabricated in a p-type doped SOI wafer (50  $\mu\text{m}$  device layer, 4  $\mu\text{m}$  oxide layer and 400  $\mu\text{m}$  handle layer). The central valve plate is 750  $\mu\text{m}$  in diameter, and radius of the inlet is 175  $\mu\text{m}$ . The gas can flow via the inlet and then outside the valve seat to the open space (Bottom-top flow). The valve plate is suspended to surrounding anchors via the flexure suspension (Figure 2.2). After mounting the piezo actuator, the valve plate can be piezoelectrically actuated to move up and down in order to open and close the seat.

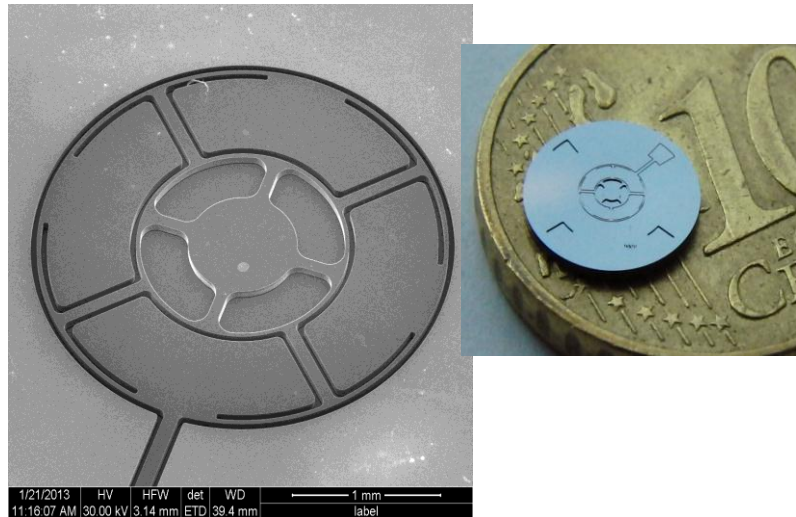


Figure 2.1: Close-up SEM micrograph (left) [6] and a photograph of the full device on top of the 10 cent coin photograph (right).

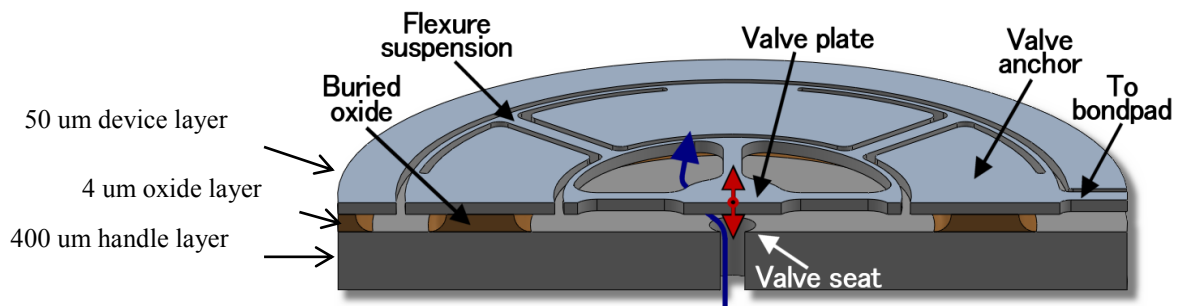


Figure 2.2: Schematic cross-sectional view of the valve design. Note that gas flow is indicated in blue arrow and valve movement is in red [6].

The fabrication of the microvalve only needs two masks and no wafer bonding is required. Twice DRIE is to etch the handle layer and the device layer, respectively (Figure 2.3 (b-c)). Buried oxide is firstly etched by 50% HF (Hydrogen Fluoride) solution, leaving some oxide underneath the valve plate (Figure 2.3 (d)). After this, vapor HF is used to remove the remaining part for the sake of preventing the valve plate from sticking on the seat by capillary forces (Figure 2.3 (e)). The microvalve chip is released from the SOI wafer by applying a torque on the breaking groove.

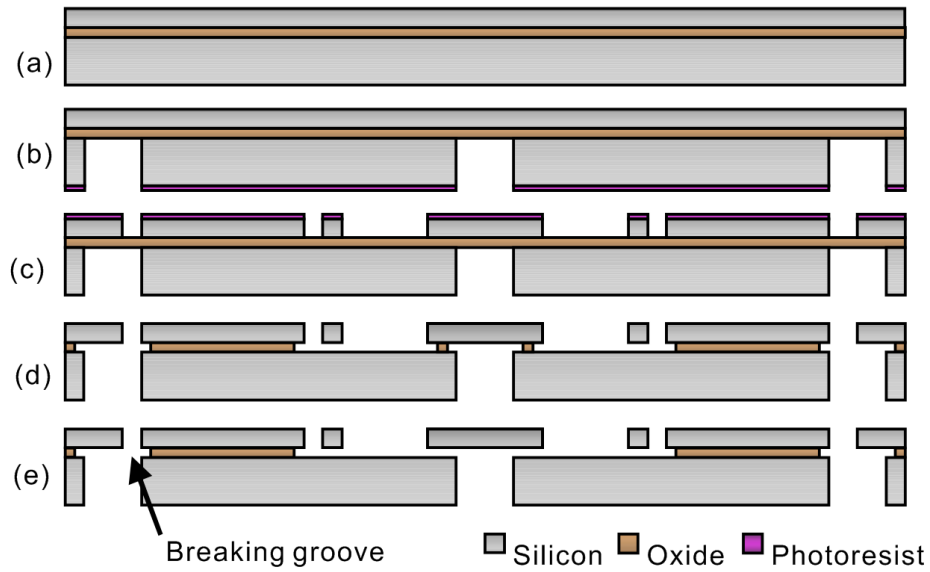


Figure 2.3: Fabrication process for the SOI-based microvalve. (a) A SOI wafer. (b) The first mask pattern and then DRIE for the inlet on the handle layer. (c) The second mask pattern, and then DRIE for the valve plate and flexure suspension on the device layer. (d) 50% liquid HF etching the oxide layer. (e) Vapor HF releases the valve plate.

## 2.3 Characterization of the piezo actuator

The piezo actuator (CMBR02 Ring bender, Noliac [11]) (Figure 2.4) will be mounted on the front side of the previously described microvalve. Note that this piezo actuator is bimorphous. Table 2.1 summarizes this piezo critical information [12].

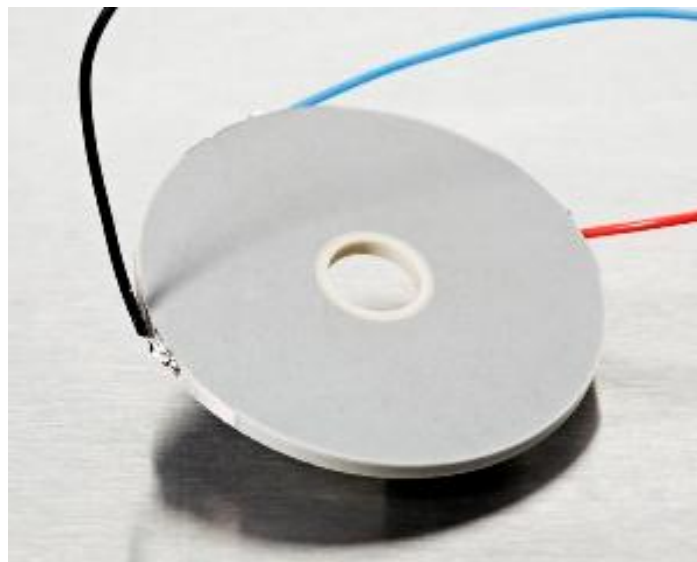


Figure 2.4: Image of Noliac CMBR02 Ring bender [11].

	Value	Tolerance
Length/outer diameter	20 mm	$\pm 0.60 \text{ mm}$
Width/inner diameter	4 mm	$\pm 0.15 \text{ mm}$
Height	1.25 mm	$\pm 0.10 \text{ mm}$
Maximum voltage	$\pm 100 \text{ V}$	
Free stroke	$\pm 28 \mu\text{m}$	$\pm 15\%$
Blocking force	16 N	$\pm 20\%$
Material	NEC57 (S1)	

Table 2.1: Specifications of Noliac CMBR02 Ring bender [12].

The Noliac piezo actuator can be controlled by a differential voltage [12]. Depending on the polarity, the bending can be both upwards and downwards. +25 V is applied to the red wire, -25 V to the black wire and a voltage  $V_{in}$  to the blue wire (e.g.,  $-25 \text{ V} < V_{in} < +25 \text{ V}$ ). In lieu of a bipolar power supply, a potential meter is used to connect the normal voltage supply which only generates the positive voltage. As a result, +50 V is applied to the red wire, 0 V to the black wire and 0—+50 V can be tuned to the blue wire (Figure 2.5). The electric capacitance of this bimorph piezo actuator is about  $2 \times 400 \text{ nF}$ , which will experience charging and discharging resulting in drift of the bending displacement when applying voltages. To minimize the effect of this, a resistance parallel connection with the piezo actuator is recommended. However, the experimental result does not show this drift, so actually this electrical connection is not applied in this experiment.

As the piezo is double-clamp mounted during the assembly, the area of mounting would significantly influence the piezo bending displacement. Thus it needs to be characterized to see the real bending displacement in the specific mounting case. In this case, 1 mm width area is clamped around the outer edge. In order to measure the central displacement, an external piezo actuator connected with a glass needle is introduced (Figure 2.6).

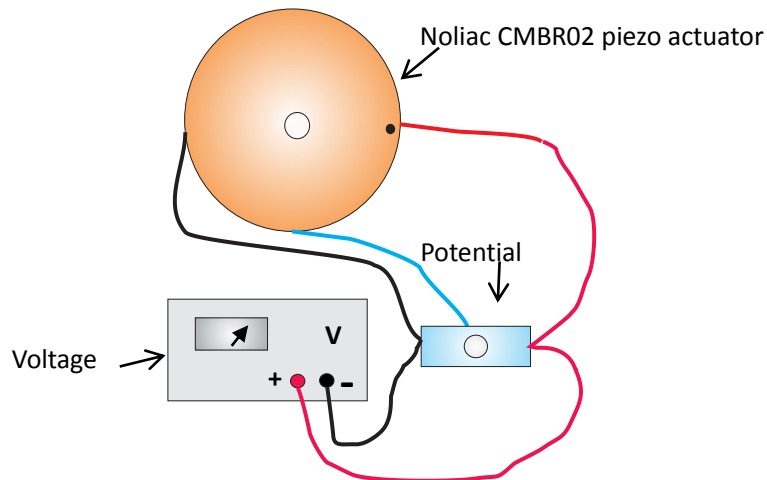


Figure 2.5: Schematic view of the electrical connection of the Noliac piezo actuator. A small black mark on the surface is used to distinguish the orientation of this Noliac piezo actuator.

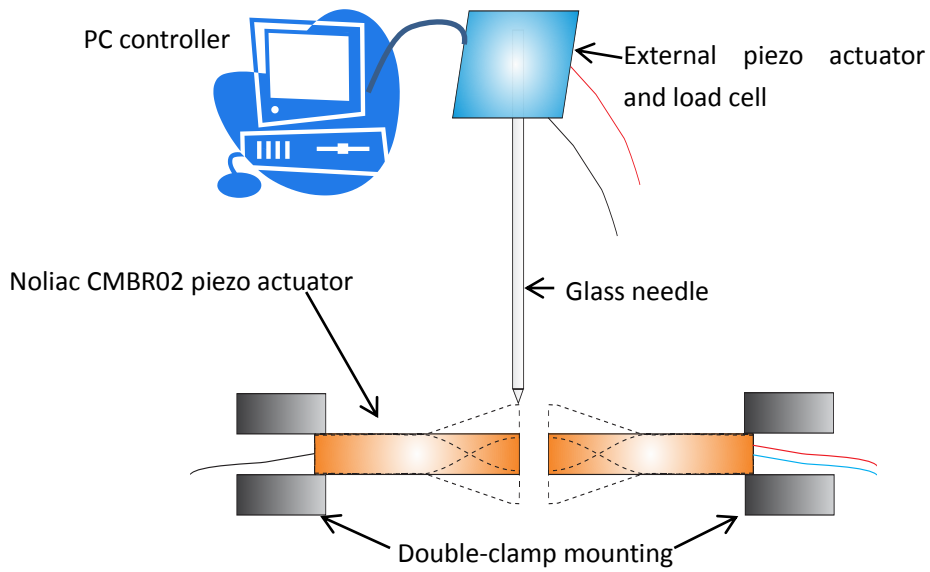


Figure 2.6: Schematic view of the setup used to characterize the piezo actuator. The dotted lines indicate the upward and downward motion of the piezo actuator. The dotted piezo actuator shapes stand for bending down and up motions.

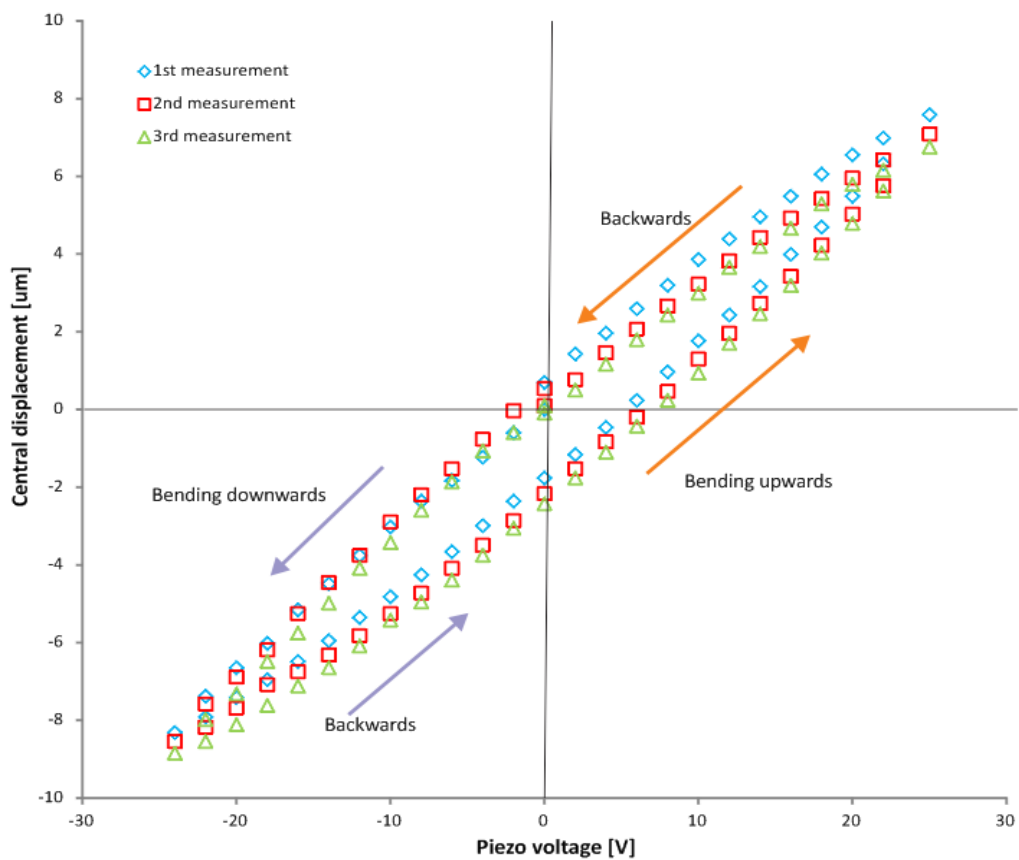


Figure 2.7: Measured Noliac CMBR02 Ring bender hysteresis. There are three times entire measurements. Purple and dark yellow arrows describe entire bending downwards and upwards routines, respectively.

The working principle is that after each voltage change applied to the Noliac piezo actuator ( $V_{pi}$ ), the external piezo actuator (PI P-603.3S2) with the glass needle can be manually tuned until the needle tip exactly touches the top surface of the Noliac piezo actuator. The glass needle is already mounted on a load cell (Futek LSM250) so that it can sense the force applied to microvalve plate. The force sensing and the displacement of the piezo actuator can be obtained in the PC controller. Theoretically, the displacement of the piezo actuator equals to the displacement of the Noliac piezo actuator. The surface with the black spot is always facing up during these three experiments. Figure 2.7 symbolizes the nonlinear hysteretic Noliac piezo actuator motion driven with 50 V peak-to-peak voltages.

## 2.4 The first assembly

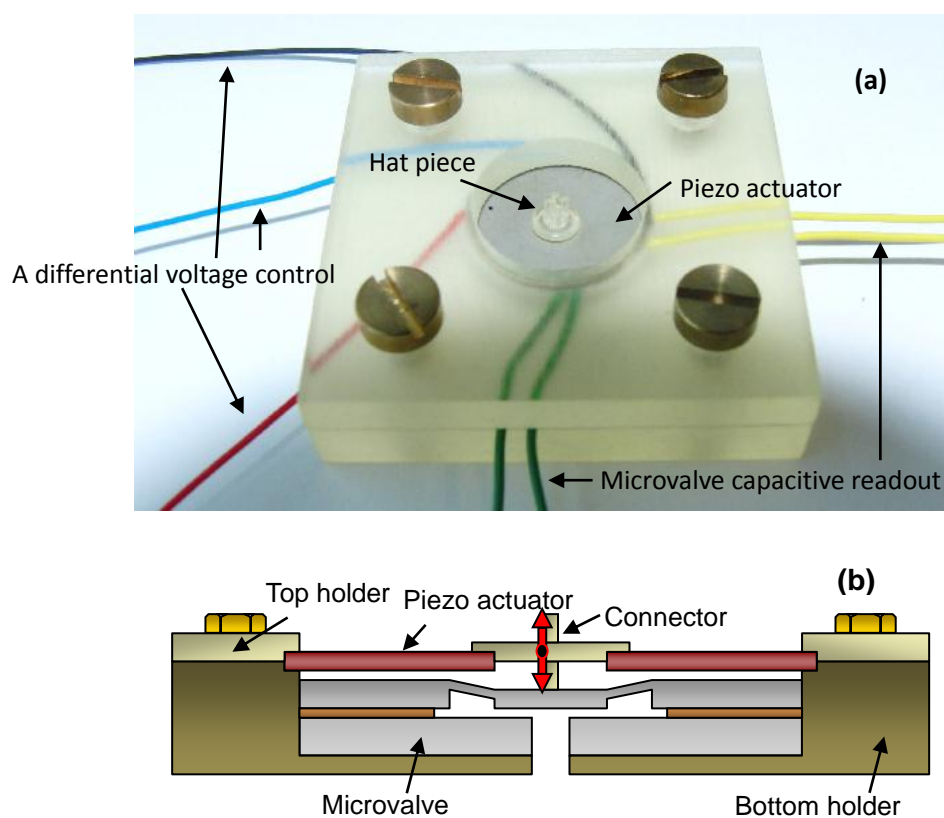


Figure 2.8: Photograph (a) of the assembled microvalve with piezo actuator and schematic cross-sectional view (b) of the whole assembly.

As the Noliac piezo actuator is much larger than the microvalve and there is a through hole in the central piezo, a connector which consists of a 3D printed hat piece (photopolymer) and an aluminum wire with 0.3 mm diameter is used to connect the piezo and the valve plate. The top and bottom holder are fabricated by 3D print (Objet Eden 250). Firstly, the top holder, the piezo actuator and the connector are glued together, and also the valve and the bottom holder are mounted (Loctite 480). Secondly, Loctite 358 UV curing glue is used to glue the connector and the valve plate together. The most difficult part is first dropping a small amount of Loctite 358 on the



from the normally open status, and then back to the original place. Theoretically 160 V peak-to-peak voltages is applied to the piezo actuator; but in reality due to an unexpected damage of the piezo actuator after assembly, the piezo actuator only works when the piezo driving voltage is 0-80 V. Thus during the experiment, 0-80 V is applied.

## 2.6 Characterization

The microvalve is normally open, so it is actuated to close first and then open. The gas pressure is varied from 100, 200, 400 and 800 mbar. During the capacitance measurement, the capacitance measured ( $C_{meas}$ ) contains a variable capacitance  $C_{var}$  between the plate and the seat, connected in parallel to a constant parasitic capacitance  $C_{par}$  between the device and handle layer (Figure 2.34). To compensate the parasitic capacitance, a normalized capacitance  $C_n$  is defined as

$$C_n = \frac{C_{meas} - C_{par}}{C_0 - C_{par}}, \quad (Eq. 2.2)[6]$$

where  $C_{meas} = C_{var} + C_{par}$  and  $C_0$  is the initial capacitance at maximum valve-seat separation.

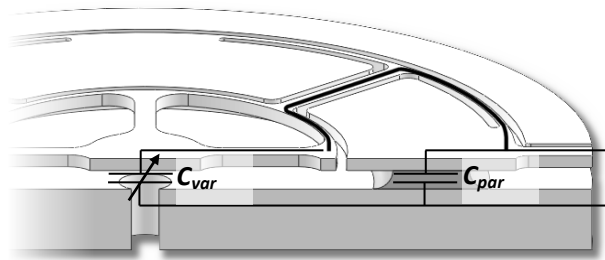


Figure 2.10: Electrical model of the capacitive microvalve [6].

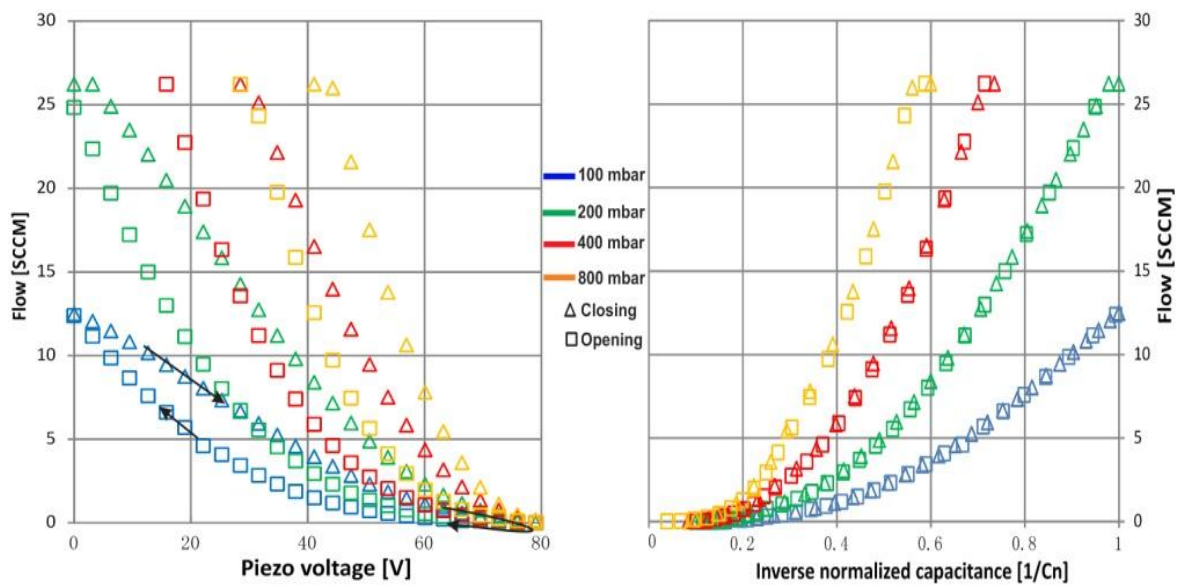


Figure 2.11: (a) Gas flow as a function of the piezo voltage with a significant hysteresis. (b) Gas flow as a function of the defined inverse normalized capacitance and the hysteresis is almost eliminated.

As the driving voltage increases, the flow rate falls, due to the reduced gap height of the valve plate and seat and reaches zero when the valve is completely closed. The closing voltages are all observed around 80 V (Figure 11 (a)). Hysteresis of the piezo actuated microvalve has been reported in many studies [7-9, 13-15]. Likewise, an evident hysteresis can be seen when the gas flow is used as a function of the piezo voltage (Figure 2.11 (a)), whereas the hysteresis is nearly circumvented when the gas flow is functionalized by the inverse normalized capacitance (Figure 2.11 (b)). Specifically, when under 200, 400 and 800 mbar pressure, there is an over 200% difference between the closing and opening flow at the same voltage (Figure 2.11 (a)). On the other hand, the closing and opening flow rates are almost matched, and all flow rates increase smoothly and continuously when the inverse normalized capacitance goes up.

## 2.6 Conclusion

In conclusion, the piezo actuator and the microvalve are successfully assembled, and the gas flowing through this assembled device is piezoelectrically characterized by using built-in capacitance displacement sensing. However, there are still some improvements can be done for the new device based on the fact that a piezo actuator is needed to mount on the microvalve.

First of all, it is better to make the direct connection between the piezo actuator and the valve plate (e.g., without using a connector); because it can, of course, reduce the assembling difficulties first and the uncertain influence (e.g., the aluminum wire from the connector bending during the actuation). Secondly, the valve plate is too small for manually locating the glue, so the new design could have some extra places to prevent from the overflow glue. Thirdly, as the photopolymer-connector is not rigid enough, which would cause deformation; displacement of the valve plate is hard to be measured by tuning the glass needle touching the photopolymer-connector surface with the external piezo actuator and the load cell (the same measurement setup in Chapter 2.3). This is because the force generated by mutual contact would possibly deform the photopolymer-connector, resulting in external displacement. Besides, the glass needle cannot be landed on the exact center of the photopolymer-connector, because the connector center is glued with the aluminum wire which is connected to the valve plate. If the glass needle is landed on the photopolymer-connector, it has risks to damage the aluminum wire. In the new valve design, it is better that using this glass needle approach can measure the valve plate displacement.

# Chapter 3 New microvalve design

This chapter presents the design of new microvalve which includes the SOI and glass valve design, which is based on the required flow resistance. Some references about modeling the flow behavior are reviewed before determining the valve specific dimension. Then, some critical dimensions of the microvalve are analyzed by software simulation.

## 3.1 Conceptual Design

### 3.1.1 SOI wafer design

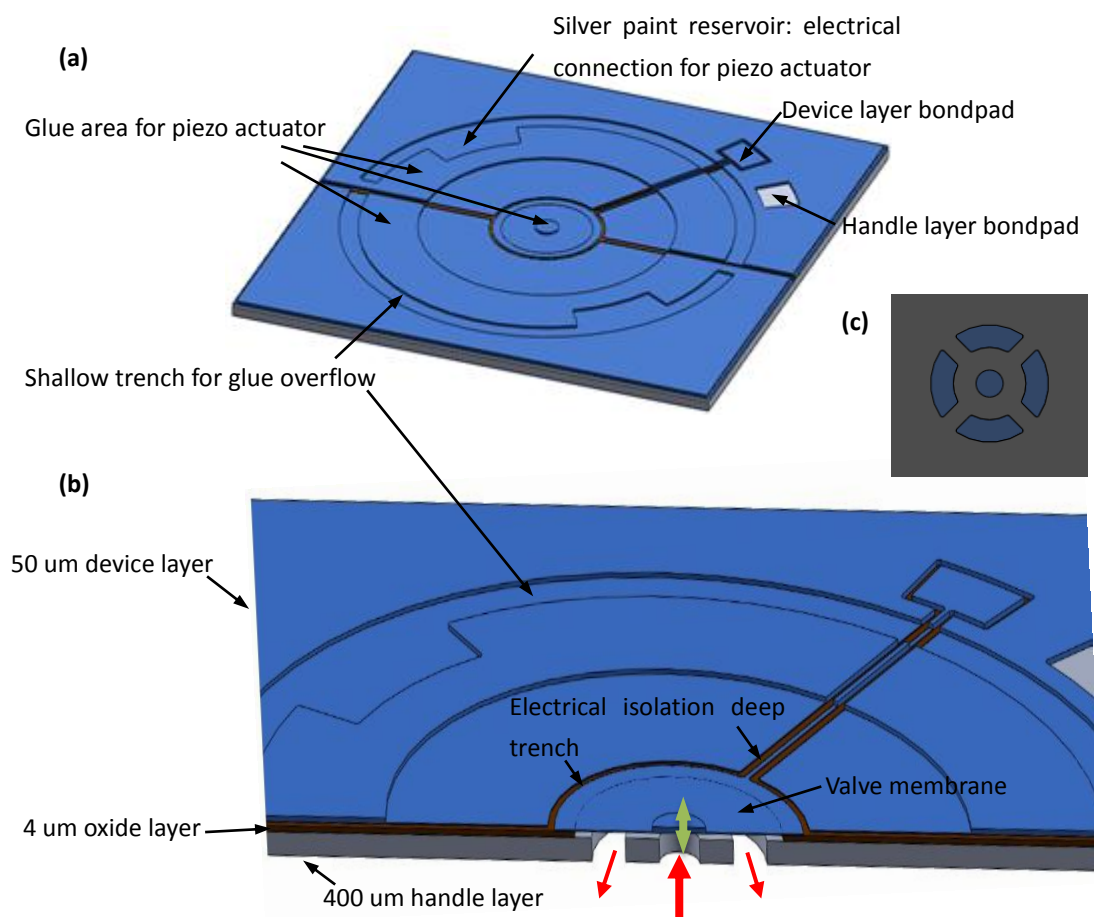


Figure 3.1: 3D structure of the new microvalve. (a) Overview of the microvalve chip. (b) Cross sectional view of the microvalve chip. The green arrow indicates the motion of valve membrane. Red arrows stand the gas flow route. (c) Bottom view of the inlet surrounded with four outlets.

New valve inlet and outlets are both designed in the handle layer, so the gas can flow from the inlet to the outlets (bottom-bottom flow). Based on the defined requirements, the new valve is designed to work under 1 bar and the volume flow through the valve needs to be higher than

100 sccm. Thus the flow resistance which is below  $6 \times 10^{10} N \cdot s/m^5$  (1 bar/ 100 sccm) is required.

Besides, considering about the overflow glue from the valve plate, there is no opening space around the valve plate; so that in fact the valve plate becomes a membrane with certain dimension (Figure 3.1 (b)). During the new design, a shallow trench is made to avoid the glue overflowing to the whole chip (Figure 3.1 (a)). Moreover, another smaller and thinner piezo actuator (T216-A4N0-273X) will replace the previous one (Noliac CMBR02 Ring bender), and it will be glued on the area which is shown in Figure 3.1 (a). As new piezo actuator has a flat surface and it can directly glue on the valve, which no need to use the connector; it makes the glass needle approach measurement (Chapter 2.3) possible. Additionally there is not any electrical connecting wire on this piezo actuator, so the place for electrical contact between the piezo actuator and the microvalve chip needs to be taken into account. On the shallow trench, there are two reservoirs for electrical connection of the piezo actuator (Figure 3.1 (a)). Silver paint can be put on one of these reservoirs, and then the electrical wires can be connected here with the bottom surface of the piezo actuator. Note that the reason for having two reservoirs is to improve the assembling possibility of success because there are two opportunities to assembly. Bondpads of the device layer and handle layer are used for capacitance readout (Figure (a)). The deep trench is for electrically isolating the valve membrane and the device bondpad during capacitance measurement (Figure 3.1 (b)). The distance between the inlet and outlet is a critical dimension of the flow model, which will be illustrated in the following sections.

### 3.1.2 Glass wafer design

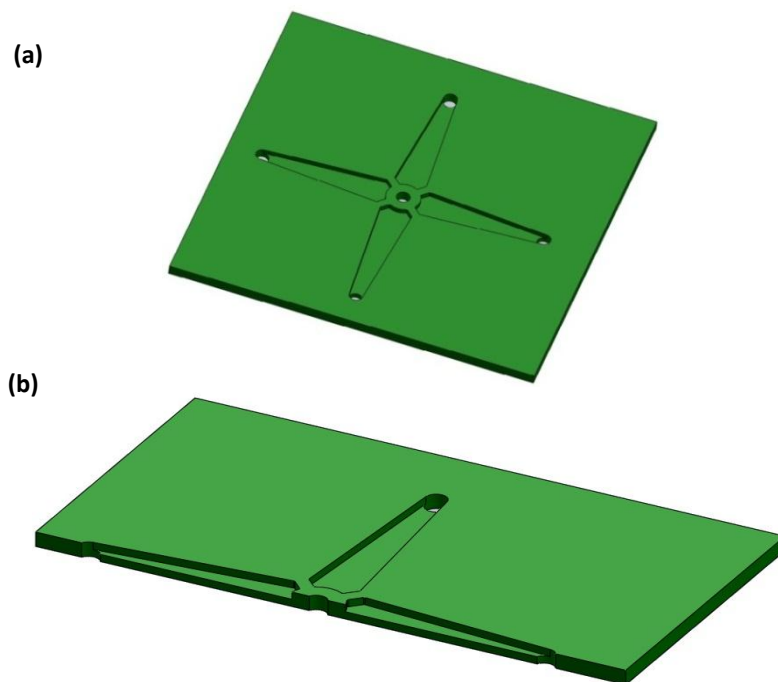


Figure 3.2: 3D structure of the valve chip in the glass wafer. (a) Top view of the glass wafer. (b) Cross section of the glass wafer.

During the measurement, a gas tube (at least a few millimeter) needs to be connected to the inlet hole ( $650\ \mu\text{m}$  in diameter), but they cannot be directly mounted together. This is because the handle layer within outlet's radius cannot be applied any external force which is generated by mounting a gas tube to the inlet orifice, would cause the valve membrane and valve seat sticking together. A possible solution could be adding an additional layer to expand the mounting area between the external gas tube and the inlet. Therefore a glass wafer which has a relatively easy fabrication process is considered (Figure 3.2).

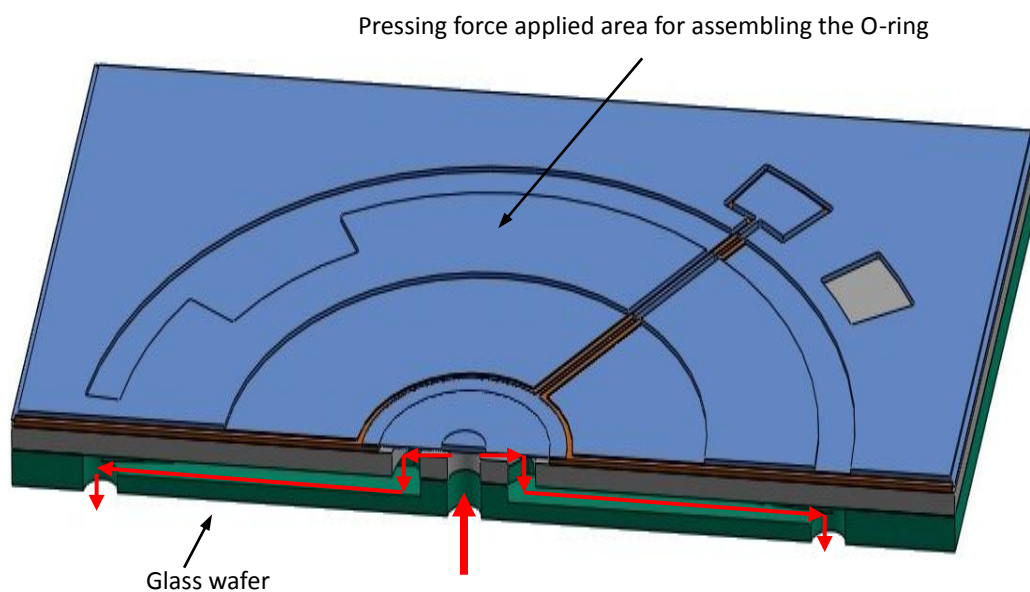


Figure 3.3: 3D structure of the anodic bonding between the SOI wafer and the glass wafer. Red arrows indicate two routes of the gas flow.

After that, anodic bonding between the SOI wafer and the glass wafer is used, and the bonding structure is shown in Figure 3.3. Also a rubber O-ring (*NBR 36624*  $10\ \text{mm} \times 1\ \text{mm}$ ) will be used to seal between the inlet and the outlet underneath the glass wafer, for which a glass wafer is required to increase the mounting area between the O-ring and the SOI wafer. Another possibility is using a good hermetic glue to localize the bonded valve chip on the chip holder.

## 3.2 Dimensioning

### 3.2.1 Reference review

In the last decade, the researchers in University of Freiburg, Germany, have done some microvalve flow modeling studies with piezoelectric membrane actuators; and the flow model used has similarities to the microvalve design in this chapter. The following paragraphs review their studies, especially in the flow model simulation. In 2006, A. Doll, M. Wischke, H. –J. Schrag, A. Geipel, F. Goldschmidtboeing and P. Woias published an analytical flow model of their micropump design (Figure 3.4) [16]. The second year, they completed their valve characterization and also presented their results [17].

They assumed a steady state, parabolic and laminar flow over the valve lip and based on the relevant fluidic mechanics [18], the fluid mechanical viscous pressure loss of the flow  $q$  through the gap of height  $h_0$  between the diaphragm and the valve lip can be estimated by

$$\Delta P_{1 \rightarrow 2} = \frac{6\eta}{\pi h_0^3} \ln\left(\frac{r_2}{r_1}\right) q \quad (Eq. 3.1)$$

where  $\eta$  is the fluidic viscosity,  $r_1$  and  $r_2$  are the inner and the outer radii of the valve seat, respectively [16].  $w = (r_2 - r_1)$  is much wider than the separation ( $h_0$ ) between the valve plate and seat. Also this mechanic modeling was performed using FEM simulation software (ANSYS 10) (Figure 3.5).

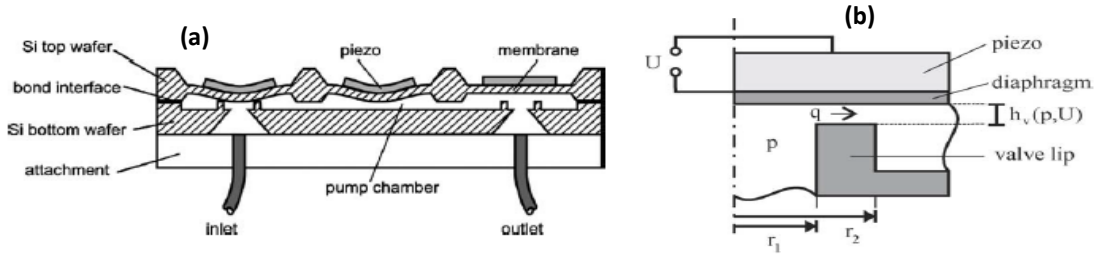


Figure 3.4: (a) Cross-section of the micropump with active valves. (b) Schematic cross-section of a valve [16].

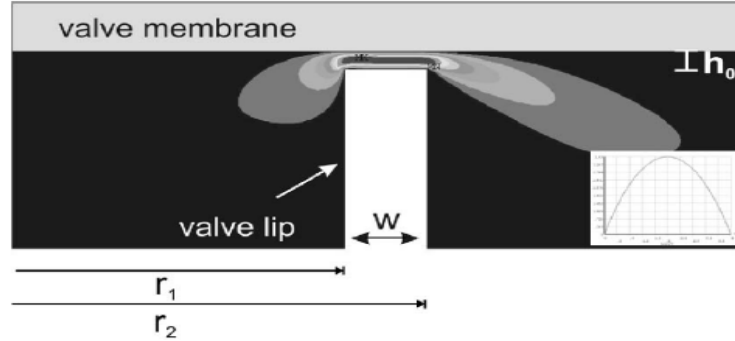


Figure 3.5: Two-dimensional numerical simulation results for the velocity distribution of the flow through the valve lip [16].

Likewise, the researchers of University of Twente, the Netherlands, also have studied the similar academic topic. In 1989, Frans C. M. van de Pol presented a radial gas flow model in his doctorate thesis work [19], which was applied in his micropump. Based on this, I. Fazal *et al.* developed Frans C. M. van de Pol's circumferential flow model in 2006 [20], and the flow resistance can be calculated by

$$R = \frac{6\mu}{s^3\pi} \ln\left(\frac{a_2}{a_1}\right) \quad (Eq. 3.2)$$

where  $\mu$  is the fluidic viscosity,  $a_1$  and  $a_2$  are the inner and the outer radii of the valve seat, respectively (Figure 3.6). The flow was assumed laminar, incompressible and fully developed.

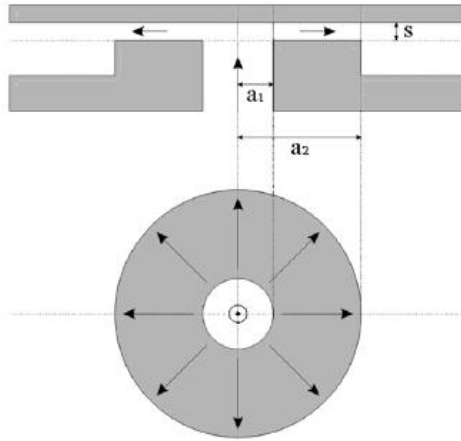


Figure 3.6: Circumferential flow [20].

### 3.2.1 Flow model simulation

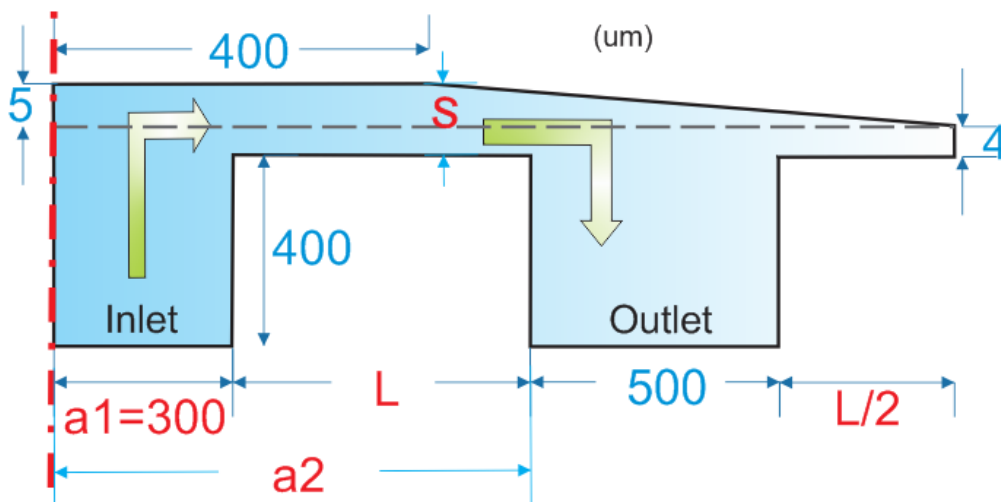


Figure 3.7: 2D symmetric inner fluid channel's cross section of the new microvalve. This valve membrane is pulled up by  $5 \mu m$ .  $4 \mu m$  is the thickness of the buried oxide layer which is etched by HF during the mass-fabrication (Chapter 4). The radius of the central stage for gluing the piezo actuator is  $400 \mu m$ , and the height of the inlet and outlet is also  $400 \mu m$  which is the handle layer. The grey dotted line indicates the valve is normally open without any motion. The green arrows show the gas flow direction inside the valve.

As Figure 3.1 depicted, the microvalve channel can be simplified as shown in Figure 3.7; and this 2D symmetric flow model is used to simulate in COMSOL Multiphysics. Separation  $s$  can be increased by piezo actuation to reduce the flow resistance, so  $L$  is the critical dimension left to determine the valve size. There is a  $L/2$  long micro channel at the end because oxide etched in HF is isotropic.  $L$  is varied from  $500, 600, 700, 800, 1000$  and up to  $1750 \mu m$ ; and the valve membrane is pulled up by a variety of displacements (from  $1$  and up to  $10 \mu m$  with  $1 \mu m$  increments). Nitrogen gas is used to simulate and the pressure drop between the inlet and outlet

is set to 1 bar. Five different positions along the channel (Figure 3.8 (b)) are analyzed. 1 bar pressure is applied in the inlet without viscous stress, and 0 bar without viscous stress in the outlet. To get flow resistance simulation in COMSOL Multiphysics, firstly mass flow is obtained, and then volume flow  $q$  can be calculated (mass flow/ density). Based on Eq. 3.2, flow resistance can be known.

Figure 3.8 illustrates how to determine the distance between the inlet and outlet ( $L$ ). As described before, the designed flow resistance should be lower than  $6 \times 10^{10} N \cdot s/m^5$ ; so the value of  $L$  which is shorter than  $800 \mu m$  is preferable (Figure 3.9). Even though when  $L$  decreasing  $R$  goes down,  $L$  cannot be made too small because it will affect the bonding area between SOI and glass wafer. If after bonding there is some voids remain in the area between the inlet and outlet, it would cause gas leakage. Therefore,  $500 \mu m$  is chosen to be length between the inlet and the outlet, which can guarantee required flow resistance and sufficient bonding area. Moreover, the COMSOL Multiphysics model simulation shows nearly linear increase of  $R$ , which matches Eq. 3.2.

According to Eq. 3.2 flow resistance  $R$  is a reciprocally cubic parabolic function of separation  $s$ . The result from COMSOL Multiphysics simulation also shows this nearly the same relationship between  $R$  and  $s$  (Figure 3.10). The data from COMSOL Multiphysics is collected from  $550 \mu m$  line position (Figure 3.8 (b)); and the data from other line position exhibits the similar curve so it is not shown here.

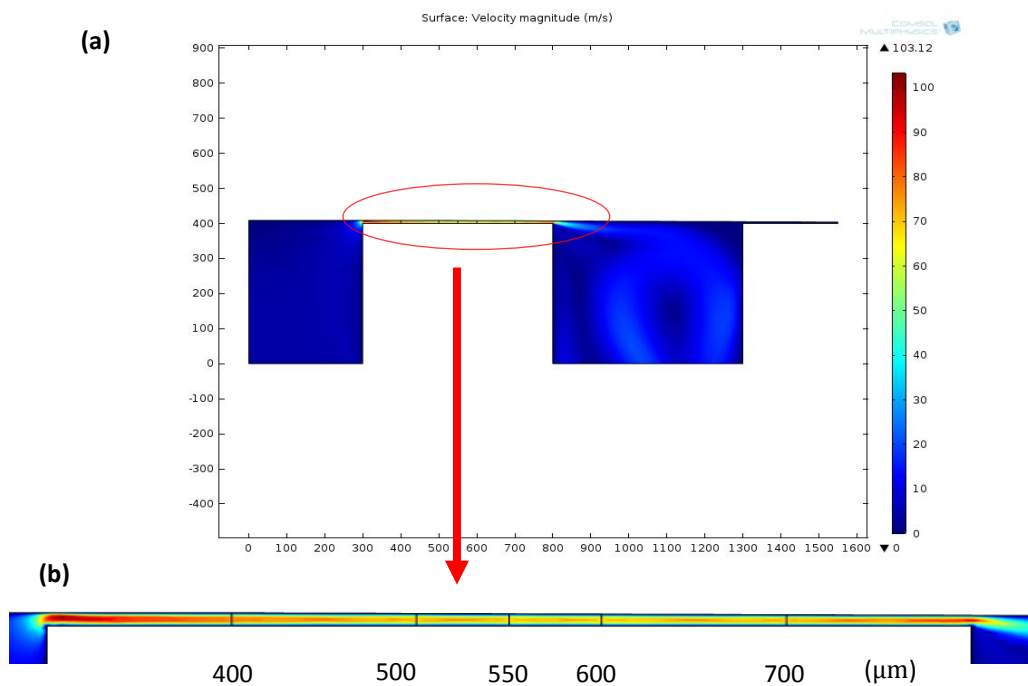


Figure 3.8: 2D simulation results for the velocity distribution of the flow through the new valve channel. (a) Overview of the simulation result. (b) Zoom-in of the simulation for the flow in the buried oxide channel.

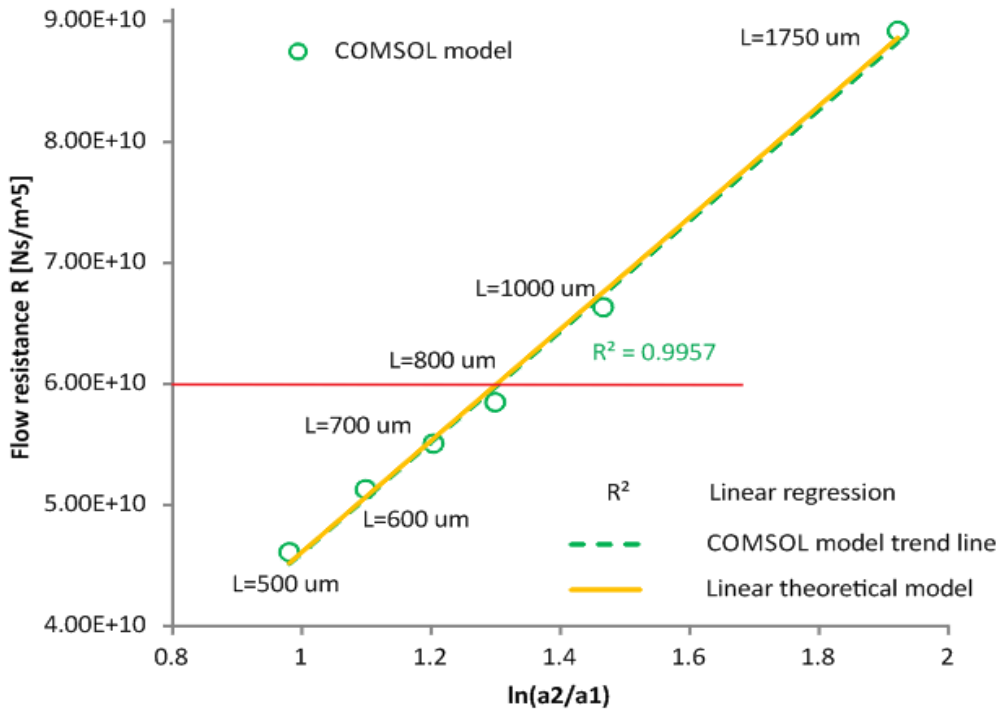


Figure 3.9: COMSOL Multiphysics simulation shows linear relation between  $\ln(a_2/a_1)$  and  $R$ . The flow resistance below the red line is required.

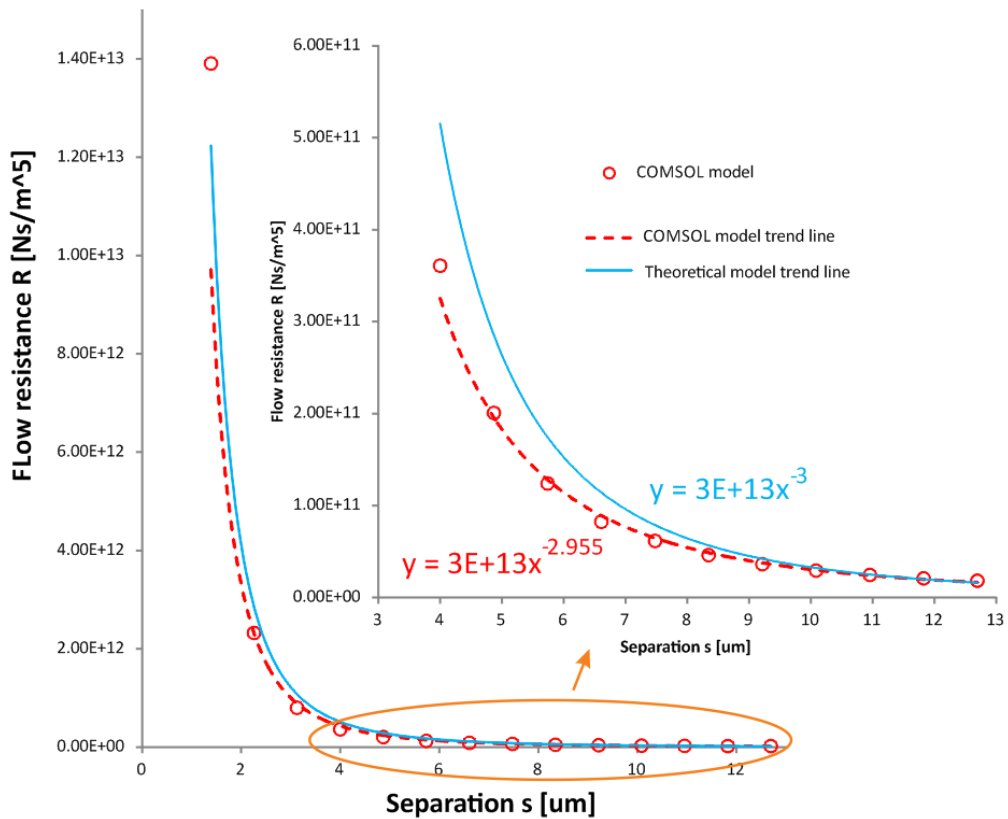


Figure 3.10: COMSOL Multiphysics simulation shows  $R$  is a nearly reciprocal cubic parabolic function of  $s$ . (a) The valve is simulated from completely closed ( $R$ =infinite large) to opened certain space. (b) Zoom-in image of the COMSOL Multiphysics result.

### 3.2.3 Valve membrane simulation

If the distance between the inlet and outlet is determined (0.5 mm), the valve membrane size can be certain (1.55 mm in radius) (Figure 3.11). As previously described, due to isotropic HF etching of oxide, the buried oxide is etched along the outlet out-axis (Chapter 2.2). Therefore during the fabrication the time control for putting the wafer into HF is of importance, if leaving the wafer in the HF bath too long, the more oxide will be etched which results in wider valve membrane (Figure 3.11 (b)). Also a small part of oxide underneath the membrane needs to be left for vapor HF etching to avoid stiction between the valve membrane and seat, using the same etching technique as the previous valve. During the design, extra  $300\ \mu\text{m}$  wide oxide is left to prevent the membrane from etching away due to the too long HF etching. The thickness of the membrane is determined by DRIE (Deep Reactive Ion Etching) process, and a homogeneous  $10\ \mu\text{m}$  thickness is to be achieved (Chapter 4).

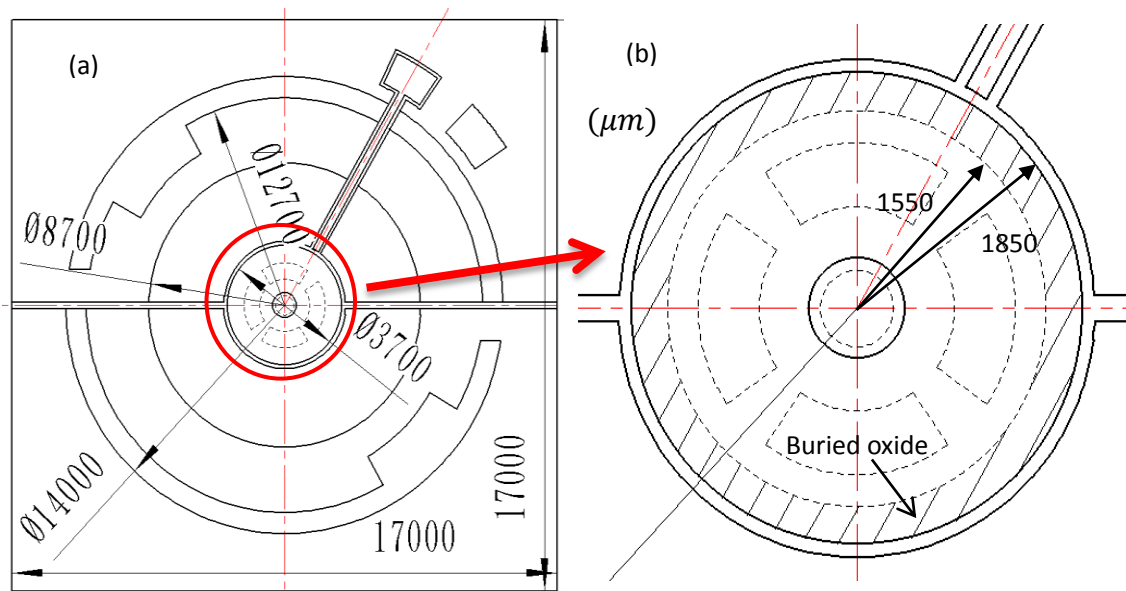


Figure 3.11: Schematic drawing of the valve chip with some critical dimensions (top view). (a) The top view of the entire valve chip. (b) Zoom-in top view of the valve membrane.

The valve membrane with 1.55 mm in radius is simulated in COMSOL Multiphysics and Figure 3.12 shows the simulation results. During the measurement, the clamping area on the piezo actuator's edge would consume a part of the blocking force of the piezo actuator; and against gas flow would also cost the available force. Therefore we choose  $-0.01\ \text{N}$  which is much smaller than the blocking force as a pulling force on the membrane to analyze the mechanical deflection during the simulation (Table 3.1) [21].  $-0.01\ \text{N}$  is perpendicularly applied on the central convex stage, and the maximum deflection ( $13.602\ \mu\text{m}$ ) of the valve membrane is on the central part. This displacement can sufficiently cover  $4\ \mu\text{m}$  buried oxide layer, which implies the valve size is eligible. Besides, the maximum stress on the valve membrane during bending is about 80 MPa, which is significantly smaller than the silicon fracture strength (1-20 GPa in single-crystal silicon). This also implies the valve with the dimension mentioned before can sufficiently survive.

Parameters	Value
Weight	0.4 g
Stiffness	$1.25 \times 10^5 \text{ N/m}$
Capacitance	4.3 nF
Rated voltage	$\pm 180 \text{ V}$
Resonant frequency	7300 Hz
Free deflection	$\pm 19.1 \mu\text{m}$
Blocked force	$\pm 2.4 \text{ N}$
Thickness	0.38 mm

Table 3.1: T216-A4NO-273X piezo actuator performance [21].

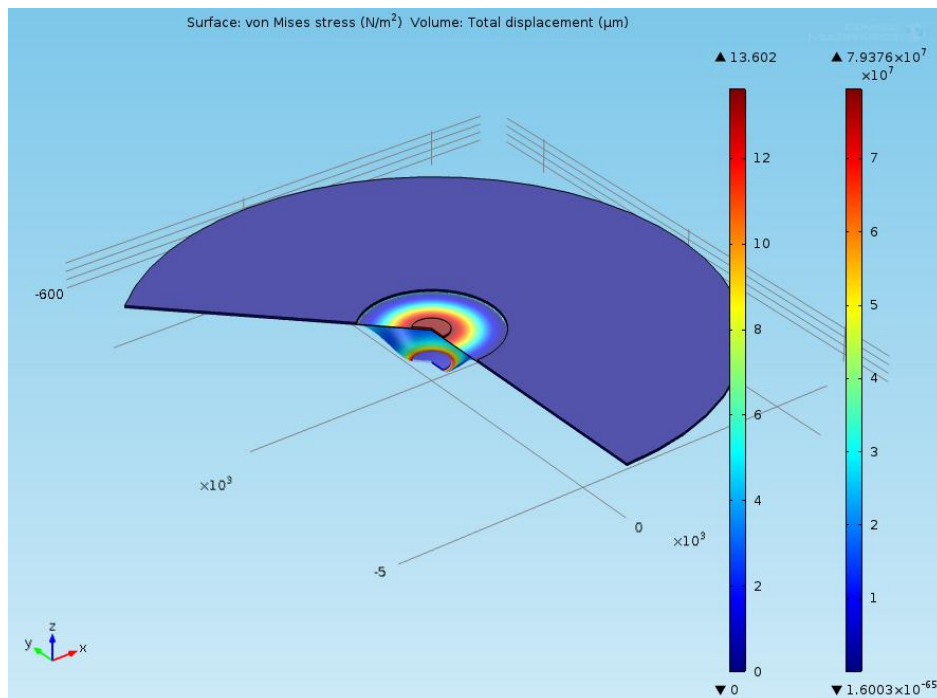


Figure 3.12: COMSOL Multiphysics simulation for the stress and the central displacement distribution of the valve membrane. The central convex stage is applied -0.01 N external force.

### 3.3 Summary

In this chapter, the new microvalve is designed based on the required fluid resistance. A glass wafer is introduced to enhance the connection between the microvalve itself and the macro flow tube for the sake of minimizing the assembling difficulties. Therefore the SOI and glass wafer design are both exhibited in this chapter. Besides, this chapter illustrates how to determine the

specific valve dimension and the flow model simulation based on the finding from F. van der Pol. *et al.* is also illustrated. Lastly, COMSOL Multiphysics mechanical simulation shows that the valve membrane is strongly able to bend to close and open the valve seat with 0.01 N, and based on that, the size of the valve can be determined.

# Chapter 4 New microvalve fabrication

---

*This chapter presents the specific microvalve fabrication steps in the SOI and glass wafer. Besides, principles of DRIE, powder blasting and anodic bonding are illustrated. A discussion of the results from DRIE, liquid HF etching and powderblasting is also given.*

## 4.1 Fabrication on the SOI wafer

### 4.1.1 Fabrication process

The SOI wafer, similar to previous fabrication, is also used to fabricate the new microvalve. Due to the design, two masks are used for the device layer and one mask for the handle layer. Figure 4.1 demonstrates the key steps for the microvalve fabrication. Firstly, the SOI wafer needs to be examined if its curvature meets the requirements because it will influence the later anodic bonding (Figure 4.1 (a)). Then one micrometer thick wet oxide  $SiO_2$  is grown on both sides of the wafer in the furnace at 1150 °C (Figure 4.1 (b)). This oxide is as a buried mask to protect the silicon area from the second DRIE (Figure 4.1 (i)), and this wet growing environment can reduce the time of oxidation. Then 0.35  $\mu m$  thick photoresist (Olin OiR 908-35, positive) is patterned on the front side. In order to make a good adhesion between the photoresist and the silicon, hexamethyldisilazane (HMDS) as a primer needs to be spin coated before photoresist. Figure 4.1 (c) shows the photoresist pattern after UV exposure and developing. When finishing the first lithography; the wafer is sent to the BHF (Buffered Hydrogen Fluoride) wet bench, and the oxide without photoresist protection is etched (Figure 4.1 (d)). Meanwhile, BHF also attack the photo resist, thus the photoresist needs longer postbake after the previous developing step (about 1 hour) to become stronger in order to survive in BHF solution. Figure 4.1 (e) shows the photoresist stripping process in 99%  $HNO_3$  solution.

After this, the same photoresist is the second coated, and then the second mask alignment becomes a critical step. Considering about the error during the alignment, the opening on the second mask is 10  $\mu m$  wider to compensate the misalignment. After UV exposure and photoresist developing, the photoresist pattern is shown in Figure 4.1 (f).

The next step is DRIE on the device layer. The deep trench is pre-etched by 30  $\mu m$ , and the remaining 20  $\mu m$  is left to etch in the second DRIE step (Figure 4.1 (g)). After the first DRIE, a cleaning step is done to remove fluorocarbon from DRIE and the remaining photoresist (Figure 4.1 (h)). The main cleaning step includes oxygen plasma treatment for 5 minutes and Piranha solution ( $H_2SO_4 + H_2O_2$ (3:1) volume %) treatment for 25 minutes at 85 °C. The second DRIE is continued to etch the shallow trench and the valve membrane (down by 40  $\mu m$ ) and completely etch the deep trench (down by 20  $\mu m$ ) (Figure 4.1 (i)). Also the same DRIE cleaning step is needed as previously mentioned. Then 50% HF is used to strip the top oxide (1  $\mu m$ ) and meanwhile the oxide of the deep trench is also over-etched 1  $\mu m$  (Figure 4.1 (j)).

To avoid oxide of the deep trench being etched on the front side in the later HF etching, the wafer is passivated by  $1\ \mu\text{m}$  thick SiRN (Silicon Rich Nitride) (Figure 4.1 (k)). Then the same photoresist used before is coated on the handle layer and the pattern is shown in Figure 4.1 (l). The exposed SiRN is etched by DRIE (Figure 4.1 (m)), and then the handle layer ( $400\ \mu\text{m}$ ) without SiRN covered is etched by DRIE continuously with different recipe (Figure 4.1 (n)). After that, the same necessary cleaning step is to get rid of the Fluorocarbon residue and the photoresist.

The buried oxide ( $4\ \mu\text{m}$ ) is etched by 50% HF solution, and an approximate ( $10\ \mu\text{m}$ ) wide oxide needs to remain for support the valve membrane during the later anodic bonding between the SOI and glass wafer (Figure 4.1 (o)). Also the technique is to prevent the valve plate sticking to the seat by the capillary force if all the buried oxide is etched by liquid HF etching. Note that it was quite successful when using this technique during the last microvalve fabrication [6]. Due to the SiRN protection on the device layer, HF only goes through the inlet and outlet from the back side. At the same time, some certain thickness of SiRN is also consumed during liquid HF etching. The remaining SiRN is removed by  $H_3PO_4$  etching (Figure 4.1 (p)), because the piezo actuator needs to mount on the silicon valve plate electrically.

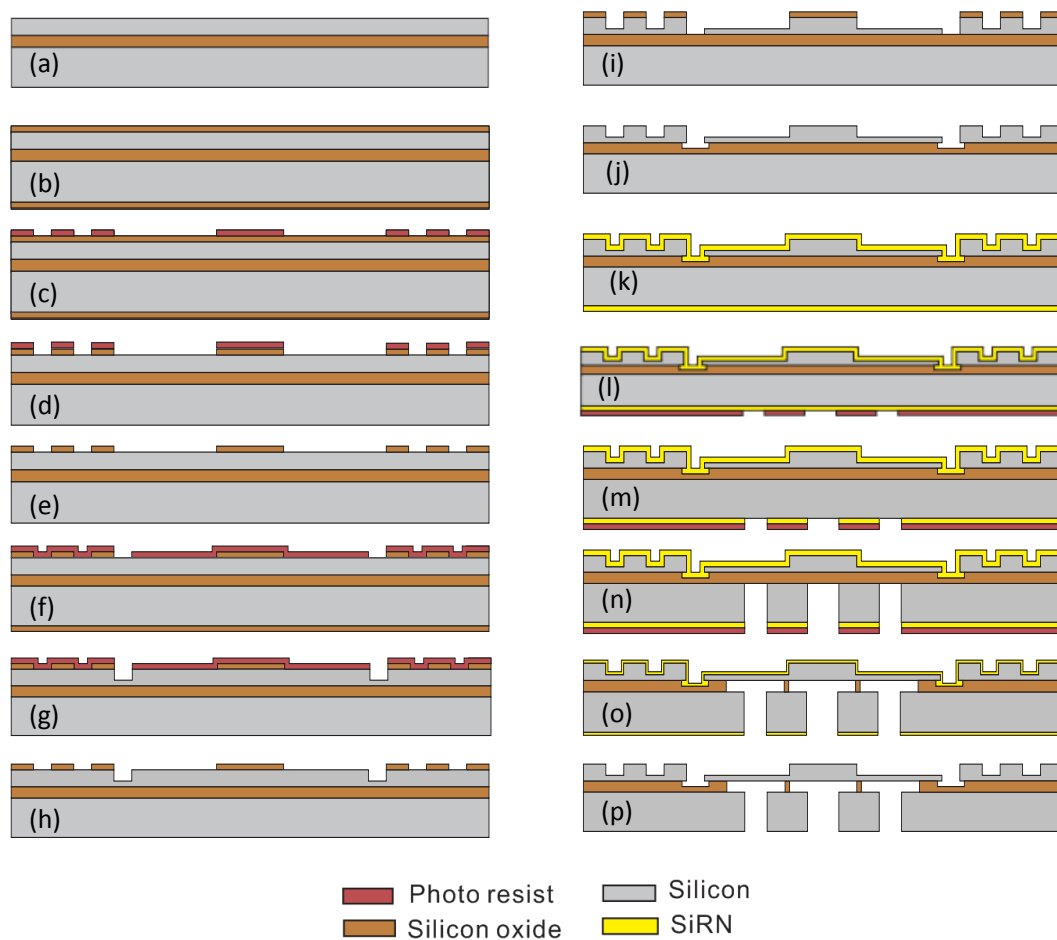


Figure 4.1: Fabrication process chart for microvalve manufactured in the SOI wafer.

## 4.1.2 Liquid HF etching experimental results

50% liquid HF solution is used to etch the buried oxide as previously described. Figure 4.2 shows the remaining buried oxide after liquid HF etching. Four small pieces of oxide (triangular shape) are the  $10\ \mu\text{m}$  wide oxide previously mentioned, and the oxide ring ( $300\ \mu\text{m}$ ) is the part which anchors the valve membrane. The etching rate of buried oxide is an important parameter during the whole device fabrication, because the remaining oxide is removed by vapor HF etching using the same technique as the previous valve (Chapter 2.2). If these four triangular oxides are remained too large, it will cost much time in vapor HF etching step. As the triangular oxide need to be left to the certain dimension, etching time control is important; so some valve structures are examined after various etching time to check how much buried oxide is left.

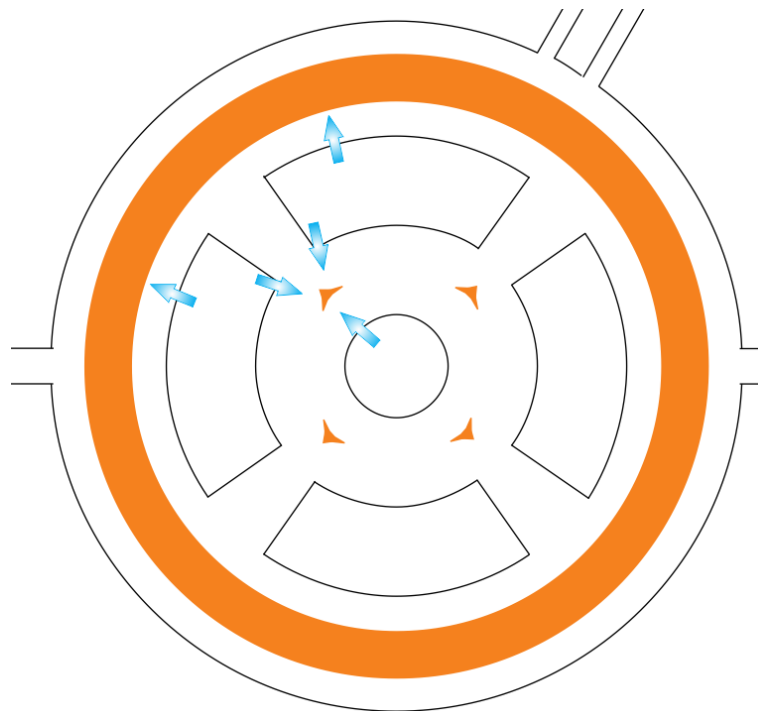


Figure 4.2: Schematic image of liquid HF etching. HF flows from the inlet and outlets. Blue arrows symbolize some critical etching directions, and yellow parts represent buried oxide which is remained after liquid HF etching.

Figure 4.3 shows after various etching time (235, 250, 260, 265 minutes, respectively), smaller oxide remain on the wafer. After each etching, the wafer is cleaned and dried, and then the valve structure is peeled off by using a tape, so the remaining buried oxide can be checked to determine the etching rate. Device layer of silicon cannot be completely peeled away from the buried oxide (Figure 4.3 (a-b)); but when etching time is longer resulted in less volume of oxide, silicon is more easily peeled off (Figure 4.3 (c-d)). The etching rate of buried oxide is about  $1\ \mu\text{m}/\text{min}$  by measuring the distance between remaining oxide and the valve inlet and outlets. Additionally, it can be observed that there are some different color rings around the valve inlet. This is probably because a very thin oxide (a few nanometers) is generated on the handle layer surface after each HF etching. Based on this, there should be additional ring after each HF etching,

but it is not observable (Figure (a-c) shows the same number of rings), possibly due to the contrast of the microscope and the real cause still needs further research.

In conclusion, liquid HF etching process can be relatively precise time controlled to etch the buried oxide in the SOI wafer. Note that the etching rate measured may be slightly different due to influences of temperature, the percentage of HF, humidity and so on.

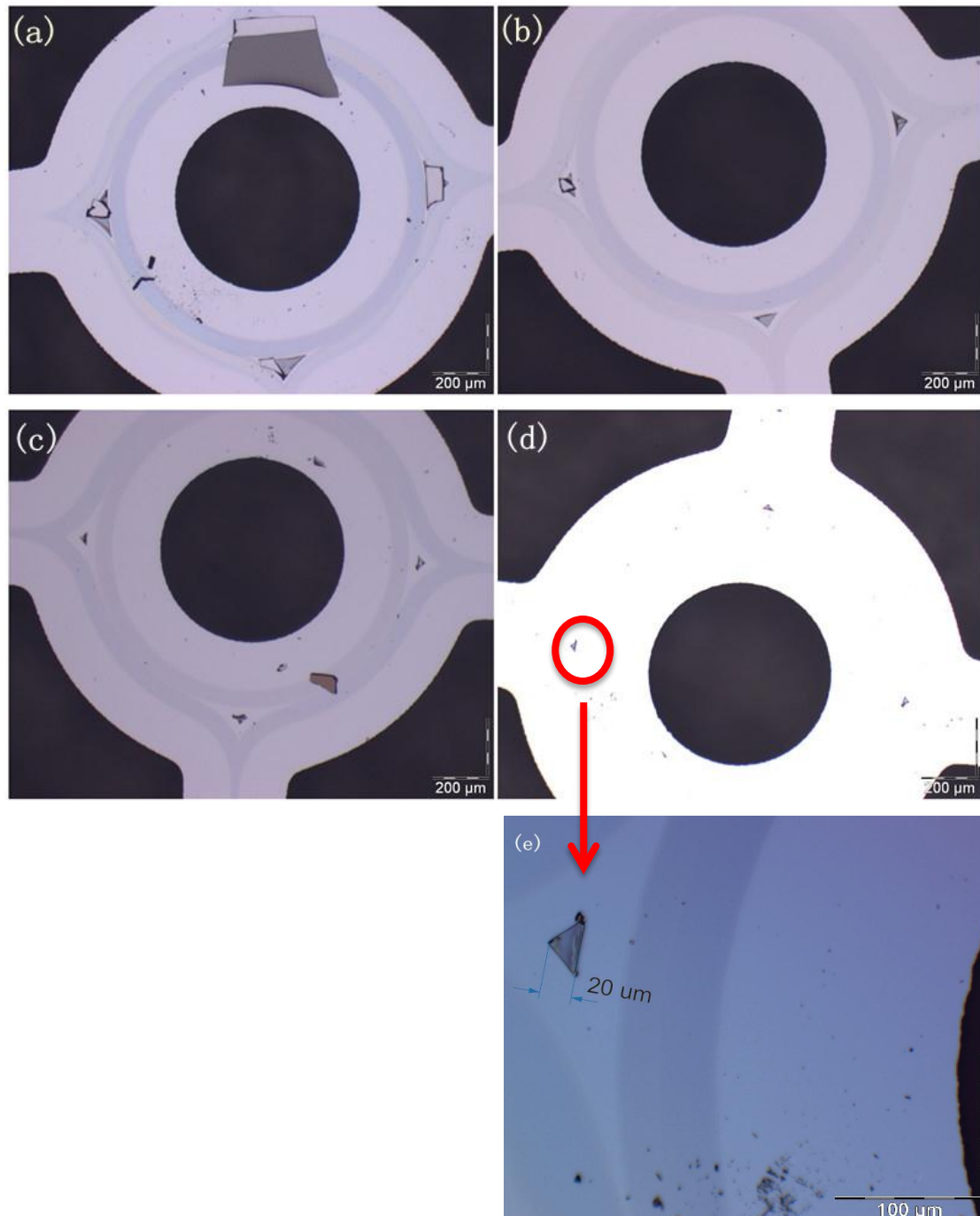


Figure 4.3: Optical microscope top views of the microvalve after various etching time (the valve membrane is peeled off). (a) After 235 minutes. (b) After 250 minutes. (c) After 260 minutes. (d) After 265 minutes. (e) Zoom-in image of one piece of triangular oxide.

### 4.1.3 DRIE experimental results

For the device and handle layer, silicon is etched using DRIE because it has high aspect ratio and relatively high etching rate ( $2 - 20 \mu\text{m}/\text{min}$ ). During the fabrication, approximately  $2.7 \mu\text{m}/\text{min}$  and  $15.3 \mu\text{m}/\text{min}$  are observed for etching the device and handle layer, respectively. In the Bosch process (named after the company which developed it),  $\text{SF}_6$  and  $\text{C}_4\text{F}_8$  gases are pulsed: a  $\text{SF}_6$  pulse etches a certain distance (a few micrometers) of silicon, but etching is not entirely anisotropic (Figure 4.4 (a)). Then  $\text{C}_4\text{F}_8$  is applied, resulting in a protective-fluoropolymer film is deposited all over the wafer. After this, the  $\text{SF}_6$  etching pulse removes the polymer film from the trench bottom by ion-assisted etching, but the polymer film on the sidewalls remains protected (even though are slightly etched by fluorine radicals) (Figure 4.4 (b)). Afterwards, the next  $\text{SF}_6$  etching step can be continued, and then a new round of the  $\text{C}_4\text{F}_8$  pulse deposits a protective layer and another  $\text{SF}_6$  etching will be repeated (Figure 4.4 (c)) [22]. It is indeed necessary to remove the fluoropolymer film totally at the end of DRIE because it can interfere with the following micromaching steps, and this is why using oxygen plasma and Piranha solution treatment as previously described.

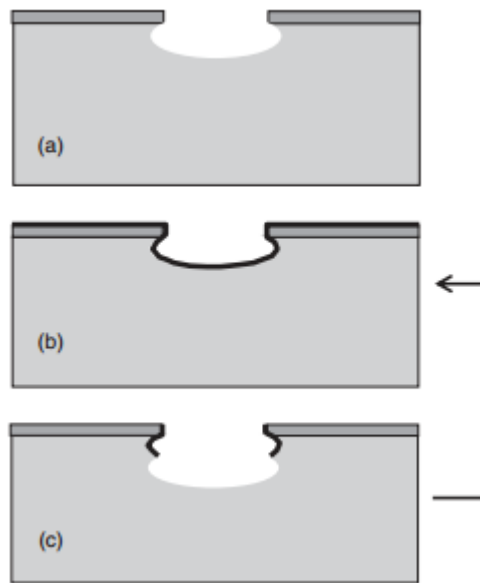


Figure 4.4: Bosch process: (a)  $\text{SF}_6$  isotropic etch step; (b) Deposition of  $\text{C}_4\text{F}_8$  passivation layer; (c) next etching step [22].

SEM (Scanning Electron Microscope) is used to analyze the result of DRIE (Figure 4.5). P-type doped silicon wafers are used to test DRIE, in order to know the dry etching rate and the quality of DRIE. Figure 4.5 (a) shows the outlet cross-section with a smooth sidewall, but some spikes are found on the bottom surface which is so-called black silicon. During DRIE, there is also a constant competition between fluorine radicals that etch and the oxygen radicals from oxygen plasma that passivate the silicon. At the certain moment, native oxide, dust, etc. will act as micromasks, and due to the directional etching, spikes will appear. These spikes contain a small piece of silicon with a thin passivating silicon oxyfluoride exterior. They will grow increasingly higher in time and exceed the wavelength of incoming light after some time. This light will be captured in the areas

between the spikes and cannot leave the silicon surface any more, which results in the etching surface turning black. The interior not only result from the native oxide, dust and so on which is already on the wafer before etching, but also silicon oxide particles from the plasma [23]. However, black silicon would not impact the microvalve because these spikes (black silicon) will be lifted off by liquid HF etching when using the SOI wafer. Figure 4.5 (b) also shows a smooth sidewall of a SOI wafer after DRIE, and a darker-color circle along the sidewall where is next to the bottom surface is observed. This circle seems inward concave, which implies the buried oxide is not reached near the sidewall, which still needs more etching time. Also the brighter-color sidewall indicates that  $C_4F_8$  passivation layer on silicon sidewall may still remain whereas less  $C_4F_8$  remain on the bottom-sidewall.

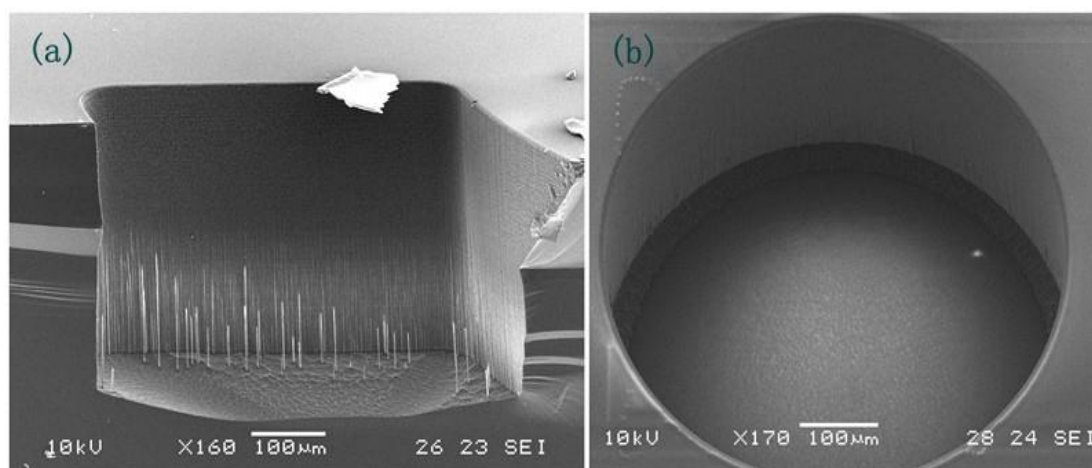


Figure 4.5: SEM micrographs of DRIE process. (a) Microvalve outlet cross-section on a dummy wafer: black silicon on the bottom surface. (b) Bottom view of the microvalve inlet on the SOI wafer: smooth sidewall and nearly bowl-shaped bottom.

After liquid HF etching and DRIE, SEM micrographs are taken to analyze fabrication results. Figure 4.6 (a-b) shows the SEM micrographs of the device layer bondpad and zoom-in bondpad beam sidewalls after DRIE, respectively. These images also show as the same straight directional sidewalls as Figure 4.5, which suggests DRIE is a reliable way to create high-aspect-ratio structures. More zoom-in silicon sidewalls are shown in Figure 4.6 (c). On the sidewalls of the high bondpad beam ( $50 \mu m$  height), layers by layers silicon pillars are found; and near the bottom sidewall, it seems fluorocarbon residuals remaining. For the lower bondpad beam ( $10 \mu m$  height), bright sidewalls are observed, probably because the fluoropolymer film is not removed yet. There is also dark bowl shape on top of the lower bondpad beam and this is probably because the second DRIE  $C_4F_8$  fluorocarbon deposition along the sidewall-shape from the first DRIE etching would influence the second DRIE  $SF_6$  etching step. But the real cause still needs further studies in the future. Figure 4.6 (d) displays the SEM micrograph of the valve membrane, and surface of the membrane seems uniform. Fig 4.6 (e) also shows the same dark bowl shape on the valve edge.

In summary, DRIE is a reliable method to create the high-aspect-ratio and tightly spaced microstructures, although it would possibly cause issues of inhomogeneity, black silicon and sidewall non-idealities.

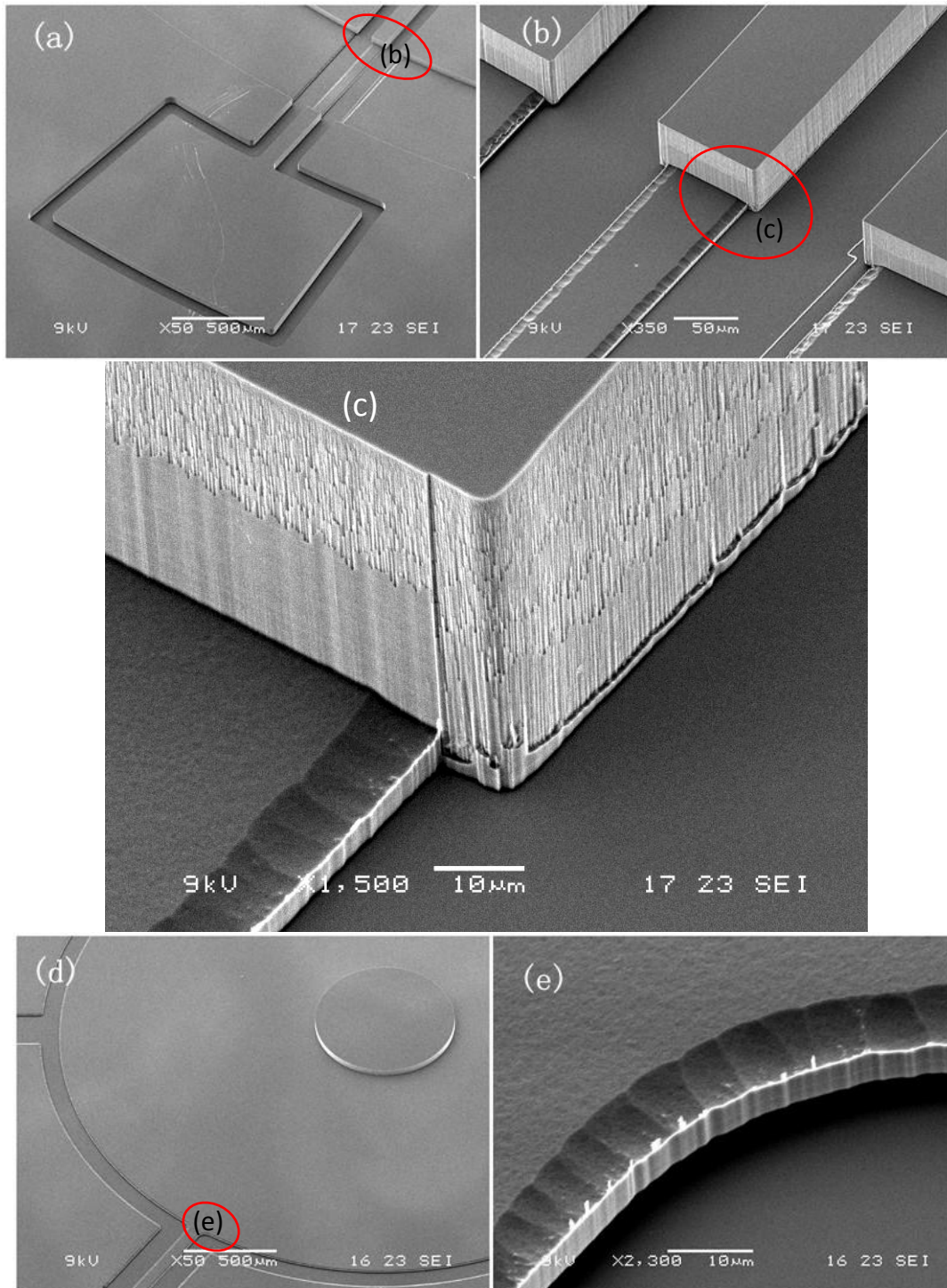


Figure 4.6: SEM micrographs of the microvalve structures. (a) Device layer bondpad. (b) Zoom-in image of the bondpad beam. (c) Zoom-in image of the bondpad beam's sidewall. (d) Valve membrane with the central convex circular stage. (e) Zoom-in image of the edge of the valve membrane.

## 4.2 Fabrication on the glass wafer

### 4.2.1 Fabrication process

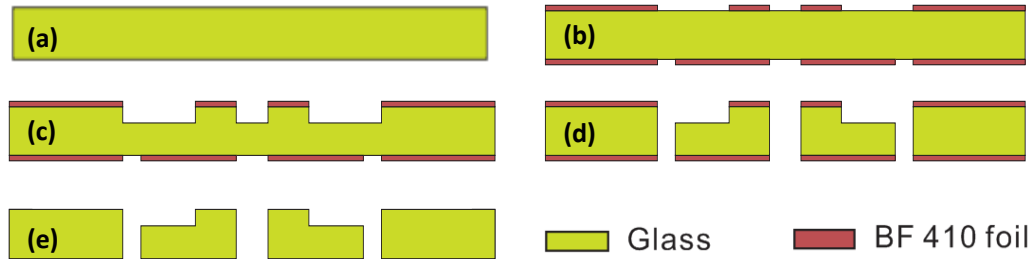


Figure 4.7: Fabrication process flow for the glass wafer.

Figure 4.7 shows the fabrication on the glass wafer. Borofloat glass wafers (4 inches,  $500 \mu\text{m}$  thick) (Figure 4.7 (a)) are used to fabricate some microchannels to lead the gas flow in and out of the microvalve. Instead of the traditional liquid photoresist coated on the substrate, BF 410 foil (negative) which is able to survive during the later powder blasting is used to pattern images on the glass wafer. The BF 410 foil is first applied on the glass wafer by a roller, which are then protected by a plain A4 carry-paper. After this, they are laminated together at  $110^\circ\text{C}$  in a laminator, and then the glass wafer is cut out of the foil to an appropriate size fitted in the UV exposure machine. After 15 seconds UV exposure, the wafer is sent to develop in  $\text{Na}_2\text{CO}_3$  solution for about 4 minutes. Likewise, the back side of the wafer is processed again to achieve the image pattern as shown in Figure 4.7 (b). Note that when laminating the foil on the back side the sticky front-side foil should be taken into account; because it will be sticky to the A4 carry-paper and then causes difficult separation issues. Therefore, a Teflon plate is used to separate the foil and the paper. Figure 4.7 (c-d) shows twice powder blasting in 33the front side and the back side, respectively. Lastly, the foil is stripped in acetone and isopropanol solution for more than 10 minutes and ultrasonic cleaning in DI (De-ionized) water for over 10 minutes (Figure 4.7 (e)).

### 4.2.2 Powderblasting experimental results

As the glass wafer will be anodic bonded with the SOI wafer, which requires a smooth bonding surface, the roughness of the glass wafer after powder blasting is worth discussing. Powder blasting is an abrasive jet machining technology which has been introduced recently compared to finer silicon micromachining, but it is still a fast directional machining technique for brittle material such as glass. Generally it is a technology in which a particle jet is directed towards a target for mechanical material removal (Figure 4.8) [24].  $\text{Al}_2\text{O}_3$  can be accelerated up to  $290 \text{ m/s}$  to bombard the target surface so that the surface can be evenly eroded. The surface roughness ( $R_a$ ) that is created with this technique is much higher (with a value of  $R_a$  between  $1 - 2.5 \mu\text{m}$ ) compared to general micromachining techniques [25]. For anodic bonding, one of the significant impacts of the rough surface is decrease of the bonding strength or even failure of bonding [26].

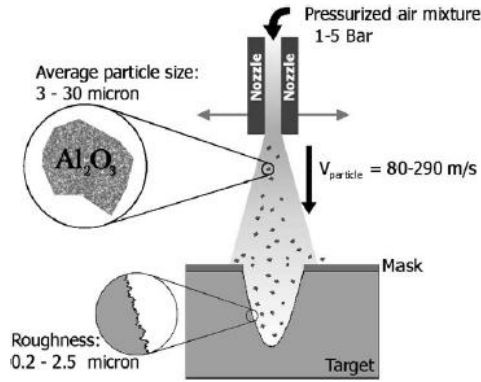


Figure 4.8: A schematic impression of the powder blast process [24].

During the powderblasting,  $29 \mu\text{m } Al_2O_3$  particles are used to erode the glass wafer. The powderblasted surface (Figure 4.9 (a)) and the sidewall of the inlet (Figure 4.9 (b)) are relatively rough. In 2009, M. C. Louwerse, H. V. Jansen, M. N. W. Groenendijk and M. C. Elwenspoek observed a glass wafer surface near to the powderblasting orifice with some irregularities that might be due to dirt particles or residuals from the powderblasting process (Figure 4.10) [27]. On the other hand, the wafer surface without powderblasting is smoother compared to the experiment of M. C. Louwerse *et al.*, which is beneficial to the later anodic bonding.

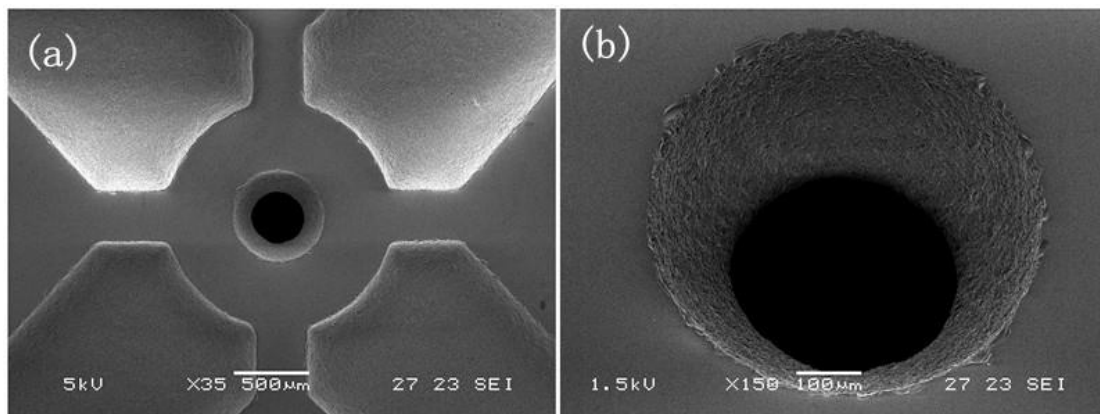


Figure 4.9: SEM micrographs of the glass wafer after powderblasting. (a) Top view of the inlet and four outlet flow channels. (b) Zoom-in image of the inlet: inclined and rough sidewall.

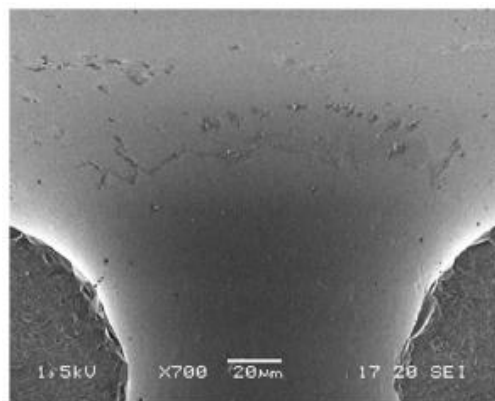


Figure 4.10: Zoom in on a nozzle inlet [27].

## 4.3 Anodic bonding

### 4.3.1 Fabrication process

Figure 4.11 exhibits the final steps of the whole fabrication. The SOI wafer and glass wafer are bonded anodically (Fig 4.11 (a)). Every valve chip is released from the bonded wafer by dicing (Figure 4.11 (c)), and a protective foil is applied to hold the diced valve chip before dicing (Figure 4.9 (b)). The last step is to use vapor HF to etch the remaining buried oxide (Figure 4.11 (e)).

Due to a vast number of particles are generated during dicing, an efficient and gentle cleaning way is required to clean the wafer. Note that an ultrasonic method cannot be used since the particle probably can flow into the valve channel, which would cause more serious problems. Here acetone with cleanroom-specialized tissue wiping is proposed based on some successful experiences.

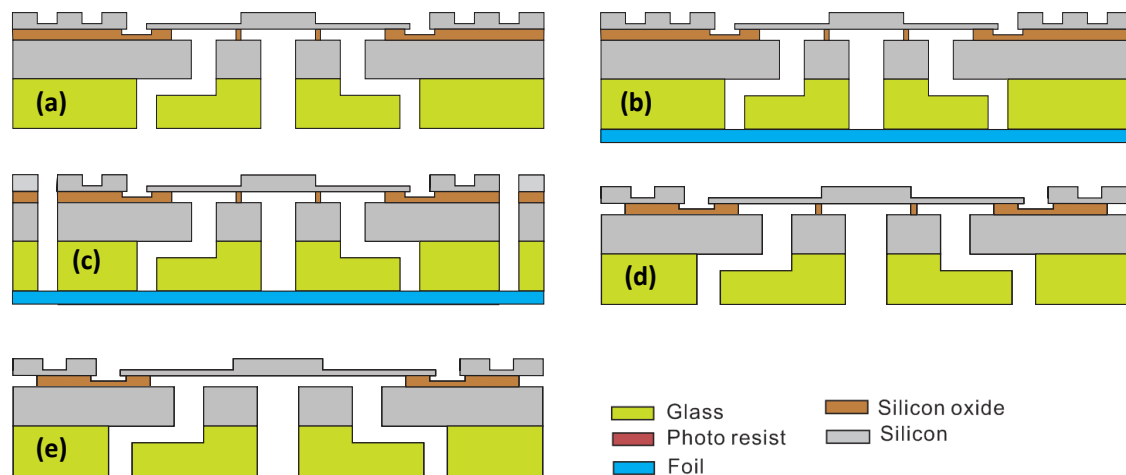


Figure 4.11: Schematics of anodic bonding and dicing steps

### 4.3.2 Anodic bonding

Silicon-glass anodic bonding is generally used for hermetic sealing and encapsulation of micromachined devices [28]. In anodic bonding, wafers to be bonded are normally heated to 300 – 500 °C and applied 400-1000 V, and then electrostatic force and the migration of ions lead to an irreversible chemical bond at the boundary layer between the silicon and glass wafers [29]. During the bonding process,  $Na^+$  ions in the glass become so mobile that they are appealed to the cathode due to an increasing temperature and voltage. Thus relatively immobile oxygen anions at the glass side of the silicon-glass interface are left, at which a space charge region is formed. This in turn creates an equivalent positive charge (image charge) on the silicon side of the silicon-glass interface resulted in a high electric field (Figure 4.12). This induced electric field drifts oxygen anions away from the  $Na^+$  depletion to the silicon surface. Therefore,

oxidation of silicon by the oxygen anions is presumed to occur and a thin oxide layer is formed at the interface, which contributes to the migration of the bonding front [30]. According to the principle of anodic bonding, magnitude of applied DC voltage, temperature, nature of surfaces to be bonded, and bonding time are critical parameters [31].

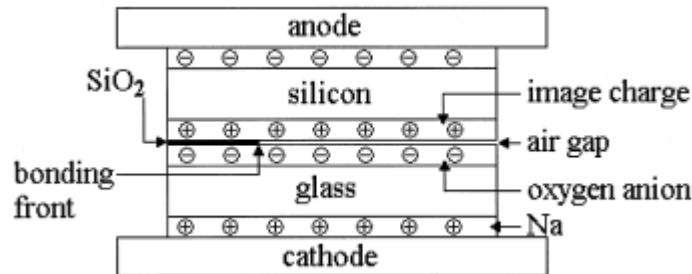


Figure 4.12: A cross-sectional view of the silicon-glass bonding pair illustrating the charge distribution during the bonding process [30].

## 4.4 Conclusion

In summary, mass micromaching of the new microvalve on the SOI and glass wafers are presented. Also, the basic theories of DRIE, powder blasting and silicon-glass anodic bonding are introduced, as well as the causes which may influence the fabrication process are discussed. Meanwhile, the processes of liquid HF etching, DRIE and powderblasting are explained, and the experimental results are analyzed.

However, due to the time issue of the whole project, the processes of vapor HF etching and anodic bonding cannot be completed. This would leave to worthwhile future work. Moreover, as the problems are found from the fabrication, relevant solutions and better process modification can be figured out in the future. For instance, for coating a foil on both sides of the glass wafer takes more time to solve the issue of the sticky foil. Twice powder blasting could change to one chemical etching step and another powder blasting step, so that twice coating foils becomes resist metal coating and only one foil laminating step.

# Chapter 5 Conclusions and recommendations

---

*This chapter presents the conclusions from the old valve assembly and its characterization, and the design and fabrication of the new microvalve are also summarized. At the end, some beneficial future works are proposed.*

## 5.1 Previous piezo control microvalve

A successful assembly between a microvalve and a piezo actuator is exhibited, capable of controlling the microvalve to characterize the gas flow (nitrogen) steadily. Built-in capacitive displacement sensing is used to characterize the flow behavior to minimize the hysteresis influence from the mounted piezo actuator. Using this method, nearly zero hysteresis effect can be reached. However, this assembling way is risky because the space left on the valve for the gluing is limited; an additional connector is introduced to connect between the valve and the piezo actuator. This results in difficult measurement of the central displacement of the valve plate.

## 5.2 New microvalve

A new design of the microvalve is presented with improving maneuverability for the next assembly, allowing easier assembly with the new piezo actuator. In the new design, piezo actuator can be mounted on the microvalve directly instead of using the additional connector to reduce the assembling difficulties. Optimization of the valve dimension is illustrated based on the required flow resistance ( $6 \times 10^{10} N \cdot s/m^5$ ). COMSOL Multiphysics simulations results of the inner valve flow channel are discussed. When the distance between the inlet and outlet is  $500 \mu m$ , the flow resistance can be obtained lower than the required one. Furthermore, mechanical properties (e.g., stress distribution and maximum bending displacement under the certain external force) of the valve membrane in COMSOL Multiphysics simulation are shown at the end. Above all, all simulations in COMSOL Multiphysics imply this new design is eligible.

A glass wafer is introduced due to the connection issue between the microvalve chip and the macro gas tube. Further, the micro-machining of the new valve on the SOI wafer and glass wafer is illustrated. In particular, timing control of the liquid HF etching is a possible way to etch a certain amount of buried oxide. Moreover, DRIE is a reliable way to obtain the high-aspect-ratio silicon structure, even though it has the disadvantages of black silicon, inhomogeneous etching and sidewall non-idealities. Additionally, powderblasting of the glass wafer has been shown that it would cause rough surface of the processed area but not on the unprocessed area, which is favorable to anodic bonding.

## 5.3 Future work

In terms of micromachining of the glass wafer, we met a problem of laminating resist foil on both sides of the wafer. During lamination of the foil on the back side with protective A4 carry-paper, the paper will permanently sticky to the front-side developed foil which is sticky. However, a plastic foil or Teflon plate in between the paper and foil can avoid this issue successfully. Also, another possible way is to use BHF etching instead of one time powder blasting. By this method, due to the isotropic etching, BHF should etch the back side of the wafer resulting in larger opening on the surface; and it would cover the distance between the inlet and outlet ( $L = 500 \mu\text{m}$ , Figure 3.2) if BHF is applied in the front side (Figure 5.1). Thus in order to apply BHF etching, a metal layer should be sputtered on the substrate as a resist foil.

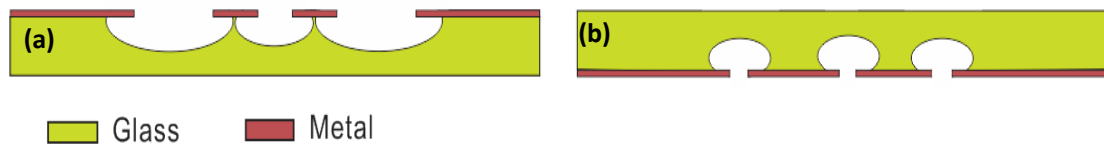


Figure 5.1: BHF isotropic etching the glass wafer. (a) BHF etches the front side and the back side is powderblasted. (b) BHF etches the back side and the front side is powderblasted.

As For the fabrication of the new microvalve on the SOI wafer, DRIE on the handle layer can be modified better, because of the inhomogeneous etching on the wafer and sidewall non-idealities. Secondly, time control of liquid HF etching needs to pay more attention as well as vapor HF etching. Moreover, anodic bonding needs to be completed in the future. For example, the factors of bonding temperature, time, applied voltage and glass wafer surface roughness after powder blasting need to be considered when processing the anodic boning.

Assembly of the new microvalve and the piezo actuator still needs to complete so that the assembled device can be characterized. More insight into this device would be beneficial. Firstly, built-in capacitive displacement sensing is still worthy trying to see if it is showing the similar behaviors as previous microvalve. Secondly, due to the new piezo actuator having a flat surface and it can mount on the valve directly by gluing, the measurement setup with the approaching needle (as the same as Chapter 2.3 described) can measure the displacement of the piezo actuator, so that we can assume the same displacement of the valve membrane bent as the piezo actuator mounted on the valve membrane. Therefore, we can obtain the relation between the gas flow and valve membrane bending displacement to see if it can verify the flow model made in Chapter 3. Thirdly, the valve response time is worth being acquainted because its medical application is supposed to monitor patients' real-time artery pressure waveform. Assume that the normal pulse rate for an adult at rest is about 60-100 bpm (Beats per Minute), so an entire heart beat waveform keeps 0.6-1 s. Also, for generating a complete heart beat cycle waveform; assume that 100 measuring points are needed. Therefore, the microvalve needs to have 6-10 ms to response in order to control the microfluidic pressure inside the finger sleeve as the same as the blood pressure.

# References

---

- [1] <http://promolding.nl/project.php?lan=uk&c=59>
- [2] M. Scheuenpflug, D. Guenther, F. Irlinger, and T. Lueth, "Microfluidic module system with piezo driven microvalve for synthesis of radiopharmaceutical products," 29<sup>th</sup> Annual International conference of the IEEE EMBS, pp. 5707-5710, Lyon, France, August, 2007.
- [3] J. Peñáz, "Photoelectric measurement of blood pressure, volume and flow in the finger," Digest of the 10th International Conference on Medical and Biological Engineering–Dresden, 1973.
- [4] <http://www.edwards.com/products/mininvasive/Pages/CCNexfinSystem.aspx?BMEye=1&WT.ac=BMEYE>
- [5] E. Chung, G. Chen, B. Alexander, and M. Cannesson, "Non-invasive continuous blood pressure monitoring: a review of current applications," *Front. Med.* 2013, 7(1): 91-101.
- [6] M. Groen, R. Brookhuis, M. van Houwelingen, D. Brouwer, J. Lotters, and R. Wiegerink, "A micro control valve with integrated capacitive sensing for ambulant blood pressure waveform monitoring," 17<sup>th</sup> International Conference on Miniaturized Systems for Chemistry and Life Sciences, MicroTAS 2013, October 2013, Freiburg, Germany, pp. 1469-1471.
- [7] P. Shao, Z. Rummler, and W. Schomburg, "Polymer micro piezo valve with a small dead volume," *Journal of Micromechanics and Microengineering*, 14 (2004) 305-309.
- [8] T. Rogge, Z. Rummler, and W. Schomburg, "Polymer micro valve with a hydraulic piezo-drive fabricated by the AMANDA process," *Sensors and Actuators, A* 110 (2004) 206-212.
- [9] X. Wu, S. Kim, C. Ji, and M. Allen, "A solid hydraulically amplified piezoelectric microvalve," *Journal of Micromechanics and Microengineering*, 21 (2001) 095003 (11pp).
- [10] M. Hu, H. Du, S. Ling, Y. Fu, Q. Chen, L. Chow, and B. Li, "A silicon-on-insulator based micro check valve," *J. Micromech. Microeng.* 14, pp. 382-387 (2004).
- [11] [http://www.noliac.com/Ring\\_benders-58.aspx](http://www.noliac.com/Ring_benders-58.aspx)
- [12] <http://www.noliac.com/Default.aspx?ID=739&NPMMode=View&ProductID=36>
- [13] M. Esashi, S. Shoji, and A. Nakano, "Normally closed microvalve and micropump fabricated on a silicon wafer," *Sensors and Actuators*, 20 (1989) 163-169.
- [14] M. Scheuenpflug, D. Guenther, F. Irlinger, and T. Lueth, "Microfluidic module system with piezo driven microvalve for synthesis of radiopharmaceutical products," 29<sup>th</sup> Annual International conference of the IEEE EMBS, pp. 5707-5710, Lyon, France, August, 2007.
- [15] T. Lemke, J. Kloeker, G. Biancuzzi, T. Huesgen, F. Goldschmidtboeing, and P. Woias, "Fabrication of a normally-closed microvalve utilizing lithographically defined silicone micro O-rings," *Journal of Micromechanics and Microengineering*, 21 (2011) 025011 (11pp).
- [16] A. Doll, M. Heinrichs, F. Goldschmidtboeing, H.-J. Schrag, U. Hopt, and P. Woias, "A high performance bidirectional micropump for a novel artificial sphincter system," *Sensors and Actuators A: Physical*, vol. 130, pp. 445-453, 2006.
- [17] A. Doll, M. Wischke, H.-J. Schrag, A. Geipel, F. Goldschmidtboeing, and P. Woias, "Characterization of active silicon microvalves with piezoelectric membrane actuators," *Microelectronic engineering*, vol. 84, pp. 1202-1206, 2007.
- [18] E. Truckenbrodt, *Fluidmechanik. 1. Grundlagen und elementare Strömungsvorgänge*

- dichtebeständiger Fluide: Springer, 1989.
- [19] Frans C. M. van de Pol, "A pump based on micro-engineering techniques," University of Twente, 1989.
  - [20] I. Fazal, M. C. Louwerse, H. V. Jansen, and M. C. Elwenspoek, "Design, fabrication and characterization of a novel gas microvalve using micro- and fine-machining," *J. Micromech. Microeng.* 16 (2006) 1207-1214.
  - [21] <http://www.piezo.com/prodbm5disk.html>
  - [22] S. Franssila, "Introduction to microfabrication," Second edition, John Wiley & Sons, Ltd, Chichester, UK, 2010.
  - [23] H. Jansen, M. de Boer, B. Legtenberg, and M. Elwenspoek, "The black silicon method: a universal method for determining the parameter setting of a fluorine-based reactive ion etcher in deep silicon trench etching with profile control," *J. Micromech. Microeng.* 5 (1995) 115-120.
  - [24] H. Wensink and M. Elwenspoek, "Reduction of sidewall inclination and blast lag of powder blasted channels," *Sensors and Actuators A* 102 (2002) 157-164.
  - [25] H. Wensink, S. Schlautmann, M. Goedbloed, and M. Elwenpoek, "Fine tuning the roughness of powder blasted surfaces," *J. Micromech. Microeng.* 12 (2002) 616-620.
  - [26] W. Choi, B. Ju, Y. Lee, J. Jeong, M. Haskard, N. Lee, M. Sung, and M. Oh, "Experimental analysis on the anodic bonding with an evaporated glass layer," *J. Micromech. Microeng.* 7 (1997) 316-322.
  - [27] M. Louwerse, H. Jansen, M. Groenendijk, and M. Elwenspoek, "Nozzle fabrication for micropropulsion of a microsatellite," *J. Micromech. Microeng.* 19 (2009) 045008 (9pp).
  - [28] M. Schmidt, "Wafer-to-wafer bonding for microstructure formation," *Proc. IEEE* 86 (8) (1998) 1574-1585.
  - [29] J. Wei, H. Xie, M. Nai, C. Wong, and L. Lee, "Low temperature wafer anodic bonding," *J. Micromech. Microeng.* 13 (2003) 217-222.
  - [30] T. Lee, D. Lee, C. Liaw, A. Lao, and I. Hsing, "Detailed characterization of anodic bonding process between glass and thin-film coated silicon substrates," *Sensors and Actuators*, 86 (2000) 103-107.
  - [31] M. Chen, X. Yi, Z. Gan, and S. Liu, "Reliability of anodically bonded silicon-glass packages," *Sensors and Actuators A* 120 (2005) 291-295.

# Acknowledgements

---

*After nine months (June 2013--February 2014), my master thesis project seems to run to an end. During this period, I have been enjoying working on this research topic, especially manufacturing the micro device in the clean room while dressing on the awesome white-protective clothing about which I was dreaming in my bachelor studies. Therefore this is the biggest reason that I chose this challenging subject at the beginning. Anyway, the result would never have turned out to be the same without the support, encouragement and assistance from the following people.*

*Maarten Groen, my daily supervisor in this assignment, with whom I have been enjoying personal and academic discussion frequently, is always in the office and clean room for giving me a strong back up. It is he who leads me to the right research direction and inspires me with new ideas. Particularly, with his great help, I obtained much useful software operating experience from modeling in SolidWorks and COMSOL Multiphysics as well as mask design in CleWin. Moreover, due to working together in the clean room, I got used to know how to fabricate the micro device in the clean room. Also, in terms of the correction of my thesis report, I received his many helpful suggestions. Thus, I am fairly grateful with his supervision and assistance, which made me complete my project better. Besides, I would also like to thank other committee members, Remco Wiegerink, Joost Lotters, and Dennis Bouwer, who gave me sufficient corrections and suggestions during the regular meeting on almost every Wednesday morning. Lastly, specially thank Professor Gijs Krijnen for his advice and being my committee. No doubt that it is impossible to carry out the results without these excellent supports.*

*Except this, I would also like to give my truly gratitude to Erwin Berenschot, Meint de Boer and Kees Ma for clean room working technique support as well as Remco Sanders for device characterization. Also, I owe my strong thanks to Niels Tas and Robert Brookhuis, who can come up with valuable solutions to the design and fabrication issues. For fabrication, my many thanks to Jarno Groenesteijn and Antoine Legrain who helped to operate DRIE as well as Johan Bomer for introduction of the powderblasting process. Their professional advice and assistance contributed a lot to my progress.*

*Without the timely support from the clean room staff, my experiments would not have been so smooth. Therefore, I would like to appreciate them all.*

*Besides, I hardly have words to express thanks to my flat mate, Bart Klaassen, sharing his philosophical insights regardless of personally or academically. Also, I express my hearty thanks to my other roommates, Selene Pelaez, Benedetta Cervone, Sylvio van Ditzhuijzen and Tobias Vermeer, who have been making my stay in the Netherlands fantastic and memorable. Furthermore, my special gratitude to my friends, Jaco Bos, Nick van der Berg, and Stefan Dekker, with whom I worked my theoretical courses' projects, which makes me keep a positive academic attitude during these two years' master studies. Additionally, I am also so grateful that have friends like, Susan Janse, Esken Meutstege, Dennis Alveringh, Jun Wang, Peng Wang, Yiyuan Zhao,*

*Peng Jin, Liang Du and Ying Tao, Lantian Chang with whom have been memorable; because I could not forget the time when we have been being together to share our different philosophical and academic perspectives which sometimes sounds crazy though. In particular, my truly thanks to Dilu Mathew, Pepijn Beekman, Peter van der Linde, Henk-Willem Veltkamp, who assisted me to revise my thesis report during the last rush days. Lastly, I am indebted to my all badminton teammates, with whom played in many Dutch cities for tournaments; which leaves me much unforgettable memory.*

*More importantly, I want to thank my beloved parents, who support my studies in the Netherlands and care me so much from thousands kilometers away. Same goes for my grandparents whose love and support have been always along with me.*

*Kai Wu  
Enschede, February 2014*